Stabilisation of HIF signalling in the epicardium extends embryonic potential and neonatal heart regeneration

Elisabetta Gamen
University of Oxford
Eleonor Price
University of Oxford
Daniela Pezzolla
University of Oxford
Carla De Villiers
University of Oxford
Mala Gunadasa-Rohling
University of Oxford
Rafik Salama
University of Oxford
David Mole
University of Oxford
Tammie Bishop
University of Oxford
Chris Pugh
University of Oxford
Robin Choudhury
University of Oxford
Carolyn Carr
University of Oxford
Joaquim Vieira
University of Oxford
Paul Riley (paul.riley@dpag.ox.ac.uk)
University of Oxford https://orcid.org/0000-0002-9862-7332

Article

Keywords: Hypoxia, heart, epicardium, development, regeneration, HIF-1α, HIF-2α, myocardial infarction, EMT, WT1.

Posted Date: June 21st, 2021

DOI: https://doi.org/10.21203/rs.3.rs-569151/v1

Stabilisation of HIF signalling in the epicardium extends embryonic potential and neonatal heart regeneration

Elisabetta Gamen[1,2], Eleonor L. Price[1,2], Daniela Pezzolla[3], Carla De Villiers[1,2], Mala Gunadasa-Rohling[1], Rafik Salama[4], David R. Mole[4], Tammie Bishop[5], Chris W. Pugh[5], Robin P Choudhury[3], Carolyn A Carr[1], Joaquim Miguel Vieira[1,2,6,*], Paul R. Riley[1,2,6,7,*]

[1]Burdon-Sanderson Cardiac Science Centre, Department of Physiology, Anatomy and Genetics, University of Oxford, Oxford OX1 3PT, UK.

[2]British Heart Foundation - Oxbridge Centre of Regenerative Medicine, CRM, University of Oxford, Oxford OX1 3PT, UK.

[3]Division of Cardiovascular Medicine, Radcliffe Department of Medicine, University of Oxford, Oxford, UK

[4] NDM Research Building, University of Oxford, Old Road Campus, Oxford, OX3 7FZ, UK

[5]Target Discovery Institute, University of Oxford, Oxford OX3 7FZ, UK.

[6]Senior author

[7]Lead Contact

[*]Correspondence: Joaquim.vieira@dpag.ox.ac.uk (JMV); paul.riley@dpag.ox.ac.uk (PRR)

Abstract

In humans, new-born infants have the ability to regenerate their heart during early life. This is modelled in the mouse, where regenerative capacity is maintained for the first week after birth but lost thereafter. Reactivation of this process holds great therapeutic potential, however, the molecular pathways that might be targeted to extend neonatal regeneration remain elusive. Here, we explore a role for hypoxia and HIF signalling on the regulation of epicardial activity which is essential for heart development and the response to injury. Hypoxic regions were found in the epicardium from mid-gestation, associating with HIF1α and HIF2α, and expression of the epicardial master regulator Wilms' tumour 1 (WT1). Epicardial deletion of *Hif1a* reduced WT1 levels, leading to impaired coronary vasculature. Moreover, targeting of the HIF degradation enzyme PHD through pharmacological inhibition with clinically approved drugs or epicardial-specific deletion stabilised HIF and promoted WT1 activity *ex vivo*. A combination of genetic and pharmacological stabilisation of HIF during neonatal heart injury led to prolonged epicardial activation, increased vascularisation, augmented infarct resolution and preserved function beyond the 7-day regenerative window. Together, these findings suggest pharmacological modulation of HIF signalling may represent a viable therapeutic strategy for treating ischaemic heart disease.

Keywords

Hypoxia, heart, epicardium, development, regeneration, HIF-1α, HIF-2α, myocardial infarction, EMT, WT1.

Introduction

The epicardium, a mesothelial sheet covering the surface of the heart, plays essential roles during cardiac development and repair. Epicardial development is evolutionally conserved from fish to mammals. In mouse, formation of the epicardium initiates at embryonic day (E) 9.5; as it expands to envelope the underlying myocardium, a subpopulation of epicardial cells undergo epithelial to mesenchyme transition (EMT) giving rise to epicardium-derived cells (EPDCs). These cells migrate into the sub-epicardial space and colonise the developing myocardium, supporting coronary vessel formation and cardiomyocyte proliferation and compaction [1]. Several transcription factors are activated in the developing epicardium, including Wilms' tumour 1 (WT1), which is instrumental in the regulation of EMT. Accordingly, when WT1 is deleted in the epicardium cells are unable to migrate into the underlying sub-epicardial region and embryos die between E14.5–E16.5 due to cardiovascular failure. Mutant embryos display oedema, accumulation of blood in the systemic veins, pericardial haemorrhaging and impaired coronary vascular development [2]. EPDCs secrete a cocktail of mitogens and chemokines, such as insulin growth factor-2 [3], angiopoietin-1 and vascular endothelial growth factor A (VEGF-A) [4], to support cardiomyocyte proliferation and regulate coronary vessel patterning. In addition to their paracrine role, EPDCs can directly give rise to many cell types, including fibroblasts [5], vascular smooth muscle cells (VSMCs) [6] and to a lesser extent endothelial cells (ECs) [7]. However, EPDC plasticity gradually decreases during embryogenesis and after birth the epicardium becomes quiescent. Embryonic genes, such as *Wt1*, are downregulated [8,9] and EMT ceases [10].

The capacity for heart regeneration after injury appears to be species-specific. Zebrafish retain the ability to regenerate their hearts throughout life, whereas adult mammals, including humans, fail to regenerate and instead replace necrotic muscle with scar tissue [11]. The loss of cardiomyocytes eventually compromises contractility of the remaining

myocardium, leading to pathological remodelling, heart failure and death [12]. By contrast, the neonatal mouse can regenerate its heart after myocardial infarction (MI) up to 7 days after birth [13] and similar regenerative capacity is evident in new-born humans [14]. In zebrafish, activation of the epicardium is an essential pre-requisite for heart regeneration [15] and in the adult mouse the epicardium becomes reactivated in response to cardiac injury to contribute to wound healing and tissue repair. Epicardial cells revert to an embryonic-like phenotype with injury; they proliferate, undergo EMT [16] and differentiate into a default fibroblast fate to stimulate ECs and the growth of coronary vessels by secreting pro-angiogenic factors, such as VEGF-A and fibroblast growth factor-2 (FGF-2) [16]. Thymosin β4 (Tβ4) pre-treatment enhances EPDC-mediated neovascularization after injury [17] and induces limited *de novo* cardiomyocyte formation by differentiation from a progenitor population of epicardial origin [8]. Upon injury *Wt1* expression, a major hallmark of the embryonic epicardial signature, is increased [18] and its transcriptional activation is epigenetically regulated by SWItch/Sucrose Non Fermentable (SWI/SNF) chromatin–remodelling complexes containing Brahma-related gene 1 (BRG1) and Tβ4 [9].

The capacity for tissue regeneration has been associated with the levels of environmental oxygen [11]. Zebrafish and neonatal mouse hearts are exposed to relatively low-oxygen or hypoxic conditions that favour the maintenance of proliferative competency of several cell types, including cardiomyocytes [19]. However, the increase in environmental oxygen after birth (in mammals) induces cardiomyocyte cell-cycle arrest[19]. Fate mapping of hypoxic cells in the adult mouse heart identified a rare population of cycling cardiomyocytes, contributing to new muscle formation[20] . More recently, exposure to hypoxia following MI was shown to induce heart regeneration in adult mice by metabolic reprogramming of cardiomyocytes leading to cell cycle re-entry[21]. Several oxygen-sensing pathways regulate cellular tolerance to hypoxia, such as the hypoxia inducible factor (HIF) family of transcription factors, among others [22]. HIF is a heterodimeric transcription factor, consisting of α and β subunits [23], with

the latter being constitutively expressed, whereas expression of the α subunit is oxygen-dependent. Under well-oxygenated conditions (i.e. normoxia), prolyl hydroxylase domain proteins (PHD1-3) hydroxylate specific conserved proline residues on the α subunit creating docking sites for the binding of the von Hippel-Lindau (VHL) protein, tagging it for proteosomal degradation [24]. When oxygen levels drop, PHD activity is inhibited, α subunit forms a heterodimer with β and translocate to the nucleus to regulate expression of its target genes, such as erythropoietin (EPO) [23] vascular endothelial growth factor, VEGF [25], and glycolytic enzymes like glucose transporter 1, GLUT-1 [26]. In human, mouse and rat there are three isoforms of the α subunit, but the best characterized are HIF-1α and HIF-2α. These bind to an identical core consensus in hypoxia response elements (HRE), but transactivate distinct, although partially overlapping, sets of genes [27,28]. Hypoxia and HIF activation are evident throughout the developing heart at E9.5, but become restricted to the outflow tract (OFT), interventricular septum (IVS) and atrioventricular (AV) cushions, following formation of the coronary vasculature at E14.5 [29]. Interestingly, HIF-1α is predominantly expressed in the myocardium, whilst HIF-2α is primarily expressed in ECs [30], and inactivation of these individual isoforms result in differential effects on cardiac development, suggesting distinct functions during cardiac morphogenesis. Embryos lacking HIF-1α die by E10.5 due to myocardial hypoplasia, reduced or absent myocardial trabeculation and a severely reduced endocardium [31,32,33]. Conversely, embryos which lack HIF-2α display variable outcomes, including extensive vascular defects, but do not exhibit major cardiac structural abnormalities [34,35]. It was also reported that the absence of HIF-1β (ARNT) in mouse is embryonically lethal and causes abnormal cardiac morphogenesis, i.e. hypoplasia and malformed endocardial cushions [36]. Disruption of the major oxygen sensor PHD2 resulted in cardiac abnormalities, such as septal defects, poorly formed trabeculae and a thin myocardial wall [37]; highlighting the importance of a tight control of hypoxia/HIF signalling for normal cardiac development.

The role of epicardial HIF signalling in mammalian heart development and regeneration remains elusive. Stabilization of HIF-1α in the epicardium of avian embryos *in vivo* and *ex vivo* inhibits EPDC migration into the myocardium through the disruption of VEGF signalling [38]. Additionally, hypoxia promotes EPDC differentiation into VSMCs through non canonical TGF-β signalling, *in vitro* [39]. Some studies have described hypoxia-mediated *Wt1* regulation. *Wt1* expression is upregulated in the heart and kidneys of rats exposed to hypoxia and an HRE binding site for HIF-1α has been identified within the promoter [40]. More recently, an additional HRE binding site for HIF-2α has been described in intron 3 of the *Wt1* gene using a neuroblastoma cell line [41]. Given that hypoxia has been implicated in regenerative responses post-MI, with correlative links to WT1 expression in the heart, we sought to investigate whether HIF signalling contributes to epicardial cell activation during heart development and following injury and as such might represent a therapeutic target for extending the regenerative window. Here, we demonstrate that the developing epicardium is hypoxic. Epicardial-specific deletion of *Hif1a* disrupted heart development with mutants displaying a significant reduction of WT1 positive cells in the epicardium and underlying myocardial layer, along with a decrease in the number of coronary vessels, indicative of defective epicardial EMT and vascularisation. In the neonatal mouse, a gradual decrease in WT1 expression, concurrent with a decrease in HIF-mediated signalling, was observed over the first week of life. Inducible genetic targeting of *Phd2* alongside pharmacological inhibition of PHDs1-3, utilising drugs already approved for other disease indications (Roxadustat, FG 4592 and Molidustat, BAY 85-3934)[42–45] stabilised HIF signalling in the injured neonatal heart. This was sufficient to maintain activation of the epicardium beyond P7, to improve cardiac remodelling and preserve function post-MI. These findings provide novel insight into the molecular mechanism regulating epicardial activation in the mouse heart and suggest that modulation of HIF signalling in the dormant epicardium may enhance cardiac repair and

150 regeneration, representing an attractive therapeutic strategy for the treatment of ischaemic
151 heart disease and heart failure.
152

153 **Results**

154 *The epicardium is hypoxic during development*

155 In order to study the role of low oxygen tension in the developing heart, we initially
156 investigated the physiological levels of hypoxia *in situ* from mid- to late gestation stages,
157 when the epicardium forms and epicardial EMT takes place. Following *in utero* treatment
158 with the marker Pimonidazole-HCl (Hypoxyprobe-1, HP1)[46] , embryonic hearts were harvest
159 at different stages, from E12.5 to E18.5 and probed with an anti-pimonidazole fluorescence-
160 conjugated monoclonal antibody (HP1), alongside immunostaining for the spatiotemporal
161 expression of HIF-1α and HIF-2α. At E12.5, when the myocardium is highly trabeculated
162 and the epicardial layer fully established, HP1 staining revealed extensive regions of
163 hypoxia, mostly in areas of dense myocardium, such as the compact wall of the
164 atrioventricular (AV) groove. At this stage, HP1 signal co-localized with the epicardial marker
165 WT1 and both HIF-1α and HIF-2α at the apex of the heart, while we observed a strong HIF-
166 1α signal in the AV groove (Figure 1a). At E14.5, extensive HP1 staining was detected in
167 areas of thicker compact myocardium, such as the interventricular septum (IVS); co-
168 localization with WT1 and HIF-1α in the epicardium, particularly in the apex and AV groove
169 regions, was also observed. HIF-2α and HP1 co-localization was found in hearts at E14.5,
170 albeit mainly in the myocardium (Figure 1b). The analysis of hearts at E16.5 and E18.5
171 revealed that the HP1 signal became progressively weaker and restricted almost exclusively
172 to WT1-expressing epicardial cells at later stages (Figure 1c, d). Similarly, HIF-1α localized
173 in discrete regions of the outermost layer of the heart, while HIF-2α immunoreactivity was
174 detected in both the epicardium (apex) and throughout the myocardium at E16.5 but
175 restricted to a few isolated myocardial cells by E18.5 (Figure 1c, d). Taken together, these
176 data suggest that WT1+ cells making up the epicardial layer of the developing heart become
177 hypoxic from mid-gestation onwards, preferentially expressing HIF-1α whereas the
178 expression of HIF-2α appeared to be mostly within the forming myocardium.

HIF-1α epicardial deletion reduces the number of Wt1+ cells and alters coronary vessel development in E16.5 embryos.

Based on the observation that the epicardium is hypoxic during mid-late gestation and that HIF-1α is mainly expressed by WT1+ cells localizing to the epicardium, we sought to investigate a functional role for HIF-1α on epicardial development. To target the expression of *Hif1α* in the epicardium, we crossed mice harbouring a tamoxifen-inducible epicardial-specific *CreERT2* driver, *Wt1*$^{CreERT2/+}$ [47], with mice in which the exon 2 of *Hif1α* gene is flanked by LoxP sites (*Hif1α*$^{fl/fl}$). Pregnant *Wt1*$^{CreERT2/+}$;*Hif1α*$^{fl/fl}$ females were injected with tamoxifen at E9.5 and E10.5, to target epicardial development, and embryos were collected at E16.5. Deletion of *Hif1α* did not alter HIF-2α expression in WT1+ cells (Supplementary Figure 1a-b). Immunostaining against WT1 revealed a significant reduction in the number of WT1+ cells in hearts from *Wt1*$^{CreERT2/+}$;*Hif1α*$^{fl/fl}$ mutants (KO) as compared to littermate controls (CTR) (Figure 2a-b). Quantification showed that the decrease in the percentage of WT1+ cells affected both the epicardial layer (Figure 2c; Mean ± SEM; CTR: 0.72 ± 0.11; KO: 0.32 ± 0.010; p=0.0268) and the myocardium (Figure 2d; Mean ± SEM; CTR: 3.96± 1.01; KO: 0.98 ± 0.25; p= 0.0461). Hearts were also probed for the endothelial marker endomucin (EMCN), to mark the endocardium and to outline the myocardial trabeculae. Mutant hearts exhibited a thinner, under-developed compact myocardium than control littermate hearts, however, no significant differences in the myocardial compaction index (Figure 2e) or in the extent of myocardial trabeculation, as assessed by fractal analysis (Figure 2f), were found between mutants and controls. Moreover, immunostaining against Ki67 (a marker of cells undergoing mitosis) did not reveal any alterations in the proliferation rate of WT1+ cells between mutants and controls (Supplementary Figure 1c-d).

The epicardium is essential for the coronary vasculature development, with loss of *Wt1* leading to absence of the coronary plexus[48]. Whole-mount immunofluorescence staining for EMCN associated with quantification using AngioTool™ software, revealed significantly

impaired coronary vessel formation following epicardial *Hif1α* deletion (Figure 2g-j). *Wt1*$^{CreERT2/+}$;*Hif1α*$^{fl/fl}$ mutant embryos presented a significant decrease in the total vessel length (microns) (Figure 2h, Mean ± SEM; CTR: 129229 ± 5509; KO: 81073 ± 10915; p= 0.0170), number of junctions (Figure 2i, Mean ± SEM; CTR: 2505 ± 63.74; KO: 1457 ± 282.1; p= 0.0223) and end points (Figure 2j, Mean ± SEM; CTR: 3422 ± 249.5; KO: 2429 ± 218.6; p= 0.0402).

During development, EPDCs are known to undergo EMT and migrate into the sub-epicardial space to support coronary vessel formation. Thus, we sought to investigate whether the lack of vascular complexity observed in the *Wt1*$^{CreERT2/+}$;*Hif1α*$^{fl/fl}$ mutant embryos was due to impaired epicardial EMT. To address this, epicardial explants were generated from E11.5 embryos from a *Rosa26*$^{+/CreERT2}$;*Hif1α*$^{fl/fl}$ mouse line, in which a tamoxifen-inducible Cre was under the control of the ubiquitous *Rosa26* promoter. Immunostaining and quantification analyses (Supplementary Figure 2a-c) confirmed that tamoxifen treatment was effective in reducing HIF-1α expression (Supplementary Figure 2b, Mean ± SEM; CTR: 0.99 ± 0.16; KO: 0.46 ± 0.12; p= 0.0397) without affecting HIF-2α levels (Supplementary Figure 2c; Mean ± SEM; CTR: 2505 ± 63.74; KO: 1457 ± 282.1; p= 0.0223). Epicardium-derived cells arising from *Hif1α*$^{fl/fl}$; *Rosa26*$^{+/CreERT2}$ mutant explants presented a cobblestone-like morphology and exhibited fewer phalloidin-labelled stress fibres as compared to control, that revealed a more spindle-like mesenchymal morphology (Figure 2k). In addition, mutant explants showed a predominant membrane alpha-smooth muscle actin (α-SMA) staining, demarcating their epithelial cell shape, whereas control cells displayed a more intense labelling of the filamentous actin cytoskeleton (Figure 2l). Consistent with our *in vivo* findings, explants derived from *Rosa26*$^{+/CreERT2}$;*Hif1α*$^{fl/fl}$ hearts showed a decreased expression of WT1 indicating impaired epicardial EMT (Figure 2m).

To test whether WT1 might be a direct target of HIF-1α we interrogated a publicly available dataset of chromatin immunoprecipitation coupled with next generation sequencing (ChIP-

seq), generated using an antibody targeting the β-subunit of the heterodimeric α-β HIF complex (i.e. HIF-1β) in the human clear cell renal cell carcinoma line 786-O[49]. The 786-O cell line has high levels of WT1 expression and is a surrogate model for active EMT and cell migration[50]. The ChIP-seq analysis revealed direct binding of HIF within intron 3 of the *Wt1* gene (Supplementary Figure 3), confirming previous findings[40].

In summary, epicardial-specific deletion of *Hif1a* significantly reduced the number of WT1+ cells, both in the epicardium and underlying myocardium, affecting coronary vessel development at E16.5. Taken together our data demonstrate that HIF regulates the expression of WT1 and associated epicardial EMT.

Stabilisation of HIF signalling enhances Wt1 expression and epicardial EMT.

We next sought to investigate whether stabilising HIF signalling under normoxic conditions is sufficient to enhance epicardial EMT. To this end, we established epicardial explants from *Rosa26*$^{+/CreERT2}$;*Phd2*$^{fl/fl}$ mice, in which cre-mediated recombination induced loss of *Phd2*, thus stabilising HIF signalling. Upon tamoxifen treatment, HIF-1α and HIF-2α expression were significantly induced in *Rosa26*$^{+/CreERT2}$;*Phd2*$^{fl/fl}$ derived explants (KO) as compared to controls (CTR) (Supplementary Figure 4a-c; HIF-1a; Mean ± SEM; CTR: 0.26 ± 0.13; KO: 0.86 ± 0.09; p= 0.0061; HIF-2a; Mean ± SEM; CTR: 0.37 ± 0.01; KO: 1.12 ± 0.15; p= 0.0027). The extent and distribution of stress fibres was then visualised with α-SMA staining, revealing an enhanced mesenchymal morphology in the mutant-derived explants (Figure 3a). In keeping, WT1 nuclear fluorescence was significantly increased in KO explants as compared to CTR (Figure 3b-c; Mean ± SEM; CTR: 158.7 ± 48.34; KO: 330.5 ± 27.26; p = 0.04).

To complement the genetic studies, we undertook a more therapeutically relevant approach by using pharmacological PHDs inhibitors to stabilise HIF signalling. Epicardial explants were generated from wildtype C57BL/6 E11.5 embryos and treated with Roxadustat (FG

4592), Molidustat (BAY 85-3934) or DMSO control. Both drugs are clinically approved, orally administered small molecules for the treatment of anaemia in patients with dialysis-dependent chronic kidney disease (CKD)[45], non-dialysis-dependent CKD[42,44] and in patients with myelodysplastic syndromes[43]. Immunostaining for HIF-1α and HIF-2α was performed (Supplementary Figure 4d-e) and stabilisation of HIF signalling upon PHDs inhibitors treatment was confirmed (Supplementary Figure 4f-g). To assess the effect of pharmacological PHD-inhibition on epicardial EMT, the proportion of mesenchymal cells was assessed by morphological evaluation. Staining with phalloidin (Figure 3d) and α-SMA (Figure 3e) showed an enhanced spindle-shape morphology with increased stress fibres, suggesting an induction of EMT in inhibitor treated-explants. Additionally, immunostaining revealed a significant increase in WT1 expression in treated explants for both drugs, as compared to control (Figure 3f-g; Mean ± SEM; Control: 1039 ± 134.9; Roxadustat: 2318 ± 438.4; Molidustat: 2500 ± 503.7; $p = 0.03$).

These data suggest that genetic perturbation and/or pharmacological inhibition of PHDs stabilised HIF signalling in the epicardium *ex vivo* to induce WT1 expression and enhance epicardial EMT.

Decline of HIF signalling is associated with epicardial quiescence in the neonatal heart.

To provide unbiased insight into Hypoxia and HIF-related molecular pathways which are differentially regulated in P1 versus P7 mouse hearts, we performed single cell RNA-seq analysis using the 10x Genomics Chromium platform and next generation sequencing. Cell clusters were visualised through uniform manifold approximation and projection (UMAP) (Figure 4a). An epicardial cell cluster (Epi) was identified based on previously described specific epicardial gene expression signatures[51] (Figure 4b). As expected, a cardiomyocyte cell cluster (CM) was underrepresented due to both low survival and size incompatibility with the FACS cell sorting [52]. Gene Ontology (GO) analysis for biological processes showed an

enrichment of hypoxia-related pathways in P1 compared to P7 epicardial cells population (Figure 4c). Accordingly, expression of well-known HIF-induced genes such as *Vegfa* and pyruvate dehydrogenase kinase 3 (*Pdk3*) was increased in P1 derived epicardial cells (Figure 4d). Conversely, the expression of *Phd2*, encoding for the main suppressor of HIF signalling, was enriched in P7 cells (Figure 4e). These findings were further confirmed by a time-course analysis of mRNA levels using ventricle lysates which revealed a marked upregulation of *Phd2* levels from P7 to adulthood (Figure 4f). Notably, the increase in *Phd2* levels coincided with a clear reduction in WT1 expression in P7 versus P1 hearts, as determined by immunostaining (Figure 4g).

To determine a causative role in the regulation of epicardial *Wt1* activity, we extended HIF signalling beyond P7 *via* the use of a genetic gain-of-function approach. *Rosa26*$^{+/CreERT2}$;*Phd2*$^{fl/fl}$ neonates were injected with a single-dose of tamoxifen at P2 to induce CRE-mediated loss of *Phd2* and stabilisation of HIF (Supplementary Figure 5a). This approach led to a reduction in *Phd2* expression levels by over 90% in *Rosa26*$^{+/CreERT2}$;*Phd2*$^{fl/fl}$ (KO) hearts compared to littermate controls (CTR; *Phd2*$^{fl/fl}$) (Mean Fold change ± SEM; CTR: 2.99 ± 0.24, n=7; KO: 0.25 ± 0.063 n=5; $p<0.0001$; Supplementary Figure 5b). Additionally, expression of the HIF target, *Glut1,* was significantly upregulated in KO hearts at P7, suggesting the activation of HIF-mediated transcription (Mean Fold change ± SEM; CTR: 0.78 ± 0.13, n=7; KO: 1.61 ± 0.20 n=5; p=0.005; Supplementary Figure 5c). Consistent with our hypothesis, WT1 expression was significantly induced in KO hearts, at both RNA (Mean Fold change ± SEM; CTR 0.84 ± 0.096, n=7; KO: 1.37 ± 0.086 n=5; p=0.003; Supplementary Figure 5d) and protein levels (Mean number of Wt1+ cells ± SEM; CTR: 9.75 ± 1.307, n=4; KO: 16.7 ± 0.3 n=2; p=0.0243; Supplementary Figure 5e). Together, these findings indicate that increased *Phd2* levels and accompanying silencing of HIF signalling lead to gradual reduction in WT1 expression and epicardial quiescence after birth and across the neonatal regenerative window.

Activation of HIF signalling improves the response to injury in non-regenerative P7 hearts

Given our findings that HIF signalling modulates WT1 expression and thus epicardial activation, we next sought to determine whether prolonged maintenance of HIF signalling would have a beneficial effect on the response to MI in the postnatal heart, beyond the first 7-days after birth. Stabilisation of HIF signalling was induced in *Rosa26*$^{+/CreERT2}$;*Phd2*$^{fl/fl}$ pups by tamoxifen injection at P2, and MI was induced by permanent ligation of the proximal left anterior descending (LAD) coronary artery in P7 mice (Supplementary Figure 5a), a time-point when the regenerative capacity of the heart is lost. Immunostaining against WT1 on transverse, apical sections from hearts collected at 4 days post-injury (dpi), revealed a widespread increase in WT1+ cells in the epicardial layer of KO, compared to CTR hearts (Figure 5a). Notably, this increase was more pronounced in the remote epicardium, than in the infarcted area, suggesting organ-wide epicardial activation analogous to that observed in the regenerating zebrafish heart[53] (Mean number of WT1+ epicardial cells ± SEM; CTR infarct zone: 51 ± 16.43; KO infarct zone: 34.14 ± 7.567, n=4, p= 0.327; CTR remote zone: 2.6 ± 1.208; KO remote zone: 15.29 ± 2.90, n=4, p= 0.0057; Figure 5b and 5c). Likewise, increased WT1 expression was detected in the myocardium, both in the infarct and remote zone of KO hearts (Mean number of WT1+ cells in myocardial layer ± SEM; CTR infarct zone: 2.22 ± 1.44; KO infarct zone: 52.09 ± 12.61, n=4, p= 0.0023; CTR remote zone: 2.625 ± 2.485; KO remote zone: 59.2 ± 16.51, n=4, p= 0.008; Figure 5d and 5e). WT1 expression in coronary endothelium has previously been described both in the developing and adult heart following MI[54], we observed extensive co-localization of WT1 and EMCN, supporting an endothelial identity for the observed incidence of myocardial WT1+ cells (Supplementary Figure 5f-g). Despite this increase in WT1+ ECs, the neovascularisation response was not substantially affected by stabilisation of HIF signalling, at 4dpi (Figure 5f). In addition, we analysed macrophage infiltration and overall cell proliferation as potential contributors to an improved response in the P7 heart, but neither were significantly altered in the absence of

335 PHD2 (Supplementary Figure 5h). Next, ventricular remodelling and scarring were assessed
336 at 21 dpi. Histological analysis of control (CTR) hearts revealed the presence of a transmural
337 scar, extending to the epicardial surface, left ventricular dilation and thinned right ventricle,
338 suggestive of pathological remodelling (Figure 5g, left panel). In the KO heart a transmural
339 scar was also observed, however the myocardium in the area of risk was comparatively
340 thicker with minimal remodelling of the left ventricle (Figure 5g, right panel), suggesting loss
341 of PHD2 may improve cardiac muscle survival post-MI. The sample size here was relatively
342 small due to technical difficulties and low survival rates associated with tamoxifen
343 administration at P2 and maternal cannibalism post injury. Therefore, to further test our
344 hypothesis that prolonged maintenance of HIF signalling has a beneficial effect on the
345 epicardium and response to MI in the postnatal heart, we explored a complementary
346 pharmacological approach recapitulating our gain of HIF-function explant studies. We
347 induced MI by LAD ligation in P7 mice and administered Roxadustat, Molidustat or DMSO
348 control (vehicle) by intraperitoneal injection, immediately after surgery and one week later,
349 to stabilise HIF signalling in the postnatal heart (Supplementary Figure 6a). Treatment with
350 either PHDs inhibitors proved effective in stabilising HIF-1α and HIF-2α, as observed by
351 immunostaining (Supplementary Figure 6b) and quantification of nuclear intensity
352 (Supplementary Figure 6c and 6d) in hearts collected at 9dpi. Moreover, this
353 pharmacological approach revealed a significant increase in epicardial WT1 expression in
354 both infarct and remote zone, in drug-treated hearts compared to controls (Figure 6a-c, %
355 of $WT1^+$ epicardial cells ± SEM; control infarct zone: 0.34 ± 0.08, n=4; Roxadustat-treated
356 infarct zone: 0.64 ± 0.13, n=4; Molidustat-treated infarct zone: 0.50 ± 0.06, control remote
357 zone: 0.075 ± 0.02, n=3; Roxadustat-treated remote zone: 0.16 ± 0.02, n=4; Molidustat-
358 treated remote zone: 0.25 ± 0.05, p = 0.03; Figure 6d-e). Similarly, an increase in WT1
359 expression in the myocardium was observed in drug-treated groups and was evidently more
360 pronounced proximal to the infarct region (% of $WT1^+$ myocardial cells ± SEM; control infarct

zone: 5.02 ± 1.34, n=4; Roxadustat-treated infarct zone: 14.32 ± 3.09, n=3; Molidustat-treated infarct zone: 7.09 ± 1.86, n=4; p = 0.03; control remote zone: 13.88± 4.96, n=4; Roxadustat-treated remote zone: 29.93 ± 6.55, n=4; Molidustat-treated remote zone: 18.61 ± 6.18, n=4, Figure 6f-g). In keeping with our previous findings using the genetic approach to target *Phd2* (Figure 5), we observed an extensive co-localization of WT1 and EMCN in the myocardium (Supplementary Figure 6e), supporting an endothelial identity for myocardial WT1+ cells. In order to determine whether the observed increase in WT1+ cells following treatment with PHD inhibitors promoted neovascularisation, immunostaining against the endothelial marker CD31 and smooth muscle marker SM-22a was performed on sections from treated and control hearts collected at 9dpi (Figure 6h-j). No significant difference in the number of vessels was observed between the different experimental groups (Figure 6k), suggesting no neovascularisation response during the initial stages post-MI. Furthermore, global and specific (WT1+) cell proliferation was assessed by immunostaining for proliferating cell nuclear antigen (PCNA), but no significant differences were observed between control and PHD inhibitor-treated animals (Supplementary Figure 6f).

In order to analyse long-term effects of HIF-stabilisation after MI, we collected hearts at 21 dpi. Interestingly, co-immunostaining and quantification of CD31 and α-SMA revealed an increase in the number of vessels in both treatment groups at this advanced stage following injury, with a more significant effect in the Roxadustat-treated mice (Figure 7a-d). To investigate whether activation of HIF signalling led to improved heart function following MI, we performed cine-MRI analysis at 21 dpi. We observed a marked reduction in left ventricular systolic function following MI in the vehicle-treated group as compared to uninjured hearts and, more importantly, a significant improvement of systolic function in the PHD inhibitor treated-groups (Figure 7e-h). MRI revealed that cardiac output (CO) and stroke volume (SV) were significantly improved in Roxadustat- and Molidustat-treated animals, with a more prominent effect in the latter group, comparable to uninjured controls

(Figure 7e-f; CO: control 10.53 ± 0.32, Roxadustat 10.14 ± 0.46, Molidustat 8.73 ±0.38, p= 0.0033. SV; control 24.37 ± 1.53, Roxadustat 22.50 ± 0.96, Molidustat 19.04 ± 0.79, p = 0.0050). Moreover, the end-diastolic volume (EDV) in the drug-treated groups was significantly improved (Figure 7h; EDV: control 33.38 ± 1.885, Roxadustat 32.26 ± 1.57, Molidustat 25.50 ± 0.82, p = 0.0011). Histological analysis by Masson's trichrome staining revealed the presence of a fibrotic scar in drug-treated animals, similar to controls (Figure 7i-j) indicating that the improved remodelling and preserved function following drug treatment were possible against a background of ensuing fibrosis. Taken together these findings suggest that treatment with PHDs inhibitors Roxadustat and Molidustat is effective in stabilising HIF signalling beyond P7, leading to an increase in WT1+ cells, improved outcome and preserved heart function following MI.

Discussion

In this study, we characterised the levels of hypoxia in the heart during mid-to-late gestation when the epicardium is fully formed. At E12.5, hypoxia was restricted to areas of compact myocardium, most significantly in the AV groove, situated close to where the coronary plexus first forms[55]. By E14.5, regions of hypoxia localised to the IVS, which is perfused later than the muscle of the free wall[56]. Finally, by E16.5 and E18.5, when the heart is sufficiently perfused by the coronaries, hypoxia was restricted to the epicardium. Further expression and distribution analysis of HIF-1 isoforms revealed a predominance of the HIF-1α isoform in $WT1^+$ cells, whereas HIF-2α appeared to be more localized to the myocardium. Hypoxia is a known promoter of EMT[57] and in the epicardium this coincided with the presence of WT1+ EPDCs. We confirmed a functional role for HIF-1α in promoting morphological changes associated with EMT by direct regulation of *Wt1* expression. Moreover, epicardial-specific deletion of *Hif1a* significantly reduced the number of WT1 expressing cells in both epicardium and myocardium, along with impaired coronary vessels in E16.5 embryos. This collectively suggests that HIF-1α mediated epicardial EMT plays an essential role in coronary vessel formation. Cre-mediated deletion of HIF-1α, induced at E9.5 and E10.5, predominantly targeted epicardial cells; however, expression of WT1 in coronary endothelium has been reported as early as E11.5[58], suggesting that the observed effects on the coronary vasculature may also be the result of aberrant HIF signalling in WT1+ ECs. However, stabilisation of HIF signalling in epicardial explant cultures under physiological oxygen levels, via genetic ablation of *Phd2*, or chemical inhibition of PHD enzymes with either Roxadustat (FG-4592) or Molidustat (BAY 85-3934), resulted in enhanced EMT and WT1 expression further confirming a role for HIF signalling in epicardial activation.

To gain insight into the molecular pathways regulated postnatally within the epicardium, we performed single cell RNA sequencing analysis comparing P1 and P7 stages and focused on the specific gene expression signature of the epicardial cell cluster. GO analysis showed

426 an enrichment of hypoxia-related pathways in P1 hearts, and the expression of well-known
427 HIF target genes showed a similar regulation. Importantly, *Phd2* expression was enriched
428 in P7 hearts, potentially contributing to epicardial quiescence during the first week of life
429 concurrent with a decrease in HIF signalling. Complete regeneration, following MI, requires
430 both the replacement of lost cardiomyocytes and the formation of new blood vessels. Given
431 the role of the epicardium during development, in promoting coronary vessel formation and
432 growth of the forming myocardium, the observed epicardial quiescence after birth likely
433 contributes to the loss of regenerative capacity. Following targeting of *Phd2*, persistent WT1
434 expression was observed in the epicardium at P7, suggesting that maintaining HIF signalling
435 after birth is sufficient to extend activation of the epicardium beyond the first week of life.
436 Genetic and pharmacological stabilisation of HIF signalling beyond P7 proved to be effective
437 in extending the regenerative window after LAD surgery, inducing the formation of new
438 vessels, reducing pathological remodelling, and preserving cardiac function against a
439 background of fibrotic repair. The observation that scarring persisted, following either
440 genetic perturbation of *Phd2* or chemical inhibition of PHDs, and yet there was significant
441 functional improvement is clinically significant, given that fibrotic repair to prevent rupture
442 after MI is considered a barrier to effective tissue regeneration[59–61]. The two pharmacological
443 inhibitors utilised in this study, Roxadustat and Molidustat, are orally administered small
444 molecules used for the treatment of anaemia in patients with dialysis-dependent chronic
445 kidney disease (CKD)[45], non-dialysis-dependent CKD[42,44] and in patients with
446 myelodysplastic syndromes[43]. Thus, there is genuine potential for repurposing these drugs
447 to treat ischemic heart disease.
448 In summary, we show that the epicardium is hypoxic at later stages of development and
449 HIF-1α is involved in epicardial activation and EMT, required to support coronary vessel
450 development. The epicardium becomes quiescent after birth with concomitant loss of HIF-
451 signalling. Genetic or pharmacological stabilisation of HIF after birth is effective in

maintaining an activated epicardium, leading to a significant improvement in cardiac remodelling and function after injury, thus representing a potential novel therapeutic target to improve cardiac regeneration following MI.

Methods

Mouse Lines

All animal experiments were carried out in accordance with the UK Home Office project license (PPL) 30/2987, PPL30/3155 and PDDE89C84 compliant with the UK animals (Scientific Procedures) Act 1986 and approved by the local Biological Services Ethical Review Process. The following mouse lines were used: Rosa$^{26+/CreERT2}$;*Hif1a$^{fl/fl}$;*, Rosa$^{26+/CreERT2}$;*Phd2$^{fl/fl}$;*. The *Wt1$^{CreERT2/+}$;Hif1a$^{fl/fl}$;* mouse line was generated by crossing *Wt1$^{CreERT2/+}$* [47] with *Hif1a$^{fl/fl}$* animals[62] for two generations. Genetically modified mouse lines used were kept in a pure C57BL/6 background. Both males and females were used in the study. For timed-mating experiments, 8-12-week-old mice were set up overnight and females checked for vaginal plugs the following morning; the date of a vaginal plug was set as embryonic day (E) 0.5. For tamoxifen-dependent gene activation, 2 doses of 40 mg/kg of body weight of tamoxifen (Sigma) were administered to pregnant dams by oral gavage, at embryonic stages E9.5 and E10.5. For neonate studies, pups were injected intraperitoneally (i.p.) with a single 10 µl dose of 20 mg/ml tamoxifen, at postnatal day (P)2, using a 25-gauge needle[63]. For hypoxia studies, pregnant females were injected i.p. with 1.5 mg Hypoxyprobe (Hypoxyprobe-1 Inc). After 2 hours, hearts from embryos were harvested and fixed.

Myocardial Infarction

All surgical and pharmacological procedures were performed in accordance with the Animals (Scientific Procedures) Act 1986 (Home Office, UK). MI was induced by permanent ligation of the left anterior descending (LAD) coronary artery in mice at postnatal day (P) 7, as previously described[64]. Wild type animals received i.p. injection of FG-4592 (Roxadustat, Selleck), BAY 85-3934 (Molidustat, Selleck) (10 mg /kg) or vehicle (DMSO), upon recovery (day 0) and 7 days later. Hearts were harvested at 4- or 9- and 21-days following ligation.

Epicardial explants

Sterile 12-well plates (Fisher Scientific), containing sterile 13-mm diameter coverslips were coated with 0.1% gelatin (Millipore) and allowed to stand for 20 minutes. The gelatin was then replaced by Dulbecco's Modified Eagle Medium (DMEM) (Sigma) containing 10% FBS (Sigma), 1% Penicillin/Streptomycin (Sigma). Hearts were isolated from E11.5 embryos and the outflow tract and atria were removed. Each ventricle was then cut in half and placed epicardial side down on the coverslip[65]. Explants were kept at 37°C/5% CO_2. 24 hours later, 1 µM of tamoxifen was added to explants. After 48 hours of culture, the explant tissue was carefully peeled off, leaving only the epicardial sheet remaining on the coverslip. For explants prepared from C57BL/6 embryos, 50 µM of FG-4592 (Roxadustat, Selleck), BAY 85-3934 (Molidustat, Selleck) or vehicle (DMSO) was added. After a total of 72 hours in culture, the media was removed, coverslips were washed briefly in ice-cold PBS and then fixed in 4% PFA at room temperature for 15 minutes. Coverslips were subsequently washed in PBS before proceeding with immunostaining.

Histological analysis

Following overnight (O/N) fixation in 2% PFA at 4°C, hearts were washed in PBS and dehydrated by passage through rising concentrations of ethanol. Samples were then washed in Butanol O/N, at RT, before being placed in molten 50:50 butanol: Histoplast paraffin wax (Fisher) at 56°C. After 1 hour the solution was replaced with 100% Histoplast paraffin wax. After several changes of 100% wax, hearts were oriented and embedded into a mould pre-loaded with paraffin. The wax was then rapidly cooled on a bed of ice and stored at 4°C. A microtome was used to cut 10µm-thick sections through the heart. Before staining, sections were first deparaffinised in Histoclear solution (Fisher), followed by rehydration through a decreasing concentration of ethanol. For Masson's Trichrome Staining, the Masson's Trichrome kit (Abcam) was used as per the manufacturer's instructions. Briefly,

508 slides were immersed in Bouin's solution for 15 minutes at 56°C. Sections were then stained
509 by serial immersion in the following solutions: Weigert's Iron Haemotoxylin solution (5
510 minutes); Biebrich Scraletacid Fuchsin (5 minutes); Aniline Blue (5 minutes);
511 Phosphotungstic/Phosphomolybdic acid solution (5 minutes) and finally 1% Acetic acid
512 solution (2 minutes). Samples were then rinsed in distilled water and dehydrated. Finally,
513 sections were cleared in Xylene and mounted using DPX mounting media.
514
515 *Immunofluorescence staining*
516 Embryos were harvested at the required embryonic stage, placed in ice-cold PBS (Sigma)
517 and the heart micro-dissected. Similarly, hearts from neonates were removed and washed
518 in ice-cold PBS. Both embryonic and neonatal hearts were fixed for 6 hours in 2%
519 paraformaldehyde (PFA; Santa Cruz Biotechnology) at 4°C and equilibrated in 30% sucrose
520 overnight at 4°C. Hearts were then placed in 50:50 30% sucrose/PBS: Tissue-Tek OCT
521 (VWR) for 30 minutes at room temperature (RT) and embedded in OCT. 10 µm-thick
522 cryosections through the heart were cut. Before use, slides were left to dry for 10 minutes
523 at RT and then washed in PBS for 5 minutes to remove the OCT. Samples were
524 permeabilised with 0.5% (sections) or 0.1% (explants) Triton X-100 in PBS (PBTr) for 10
525 minutes at RT and subsequently rinsed twice in PBS. Samples were blocked in 10% Serum,
526 1% bovine serum albumin (BSA, Merck), 0.1% PBTr for 1 hour at RT prior to incubation with
527 the primary antibodies overnight at 4°C. The following day, slides were washed three times
528 for at least 5 min in 0.1% PBTr. Samples were incubated with Alexa Fluor®-conjugated
529 secondary antibodies (1:200 dilution; Invitrogen) and 4',6-Diamidino-2-Phenylindole,
530 Dihydrochloride (DAPI; 0.1 µg/ml, Invitrogen), for 1 hour at RT, protected from light. After
531 final washes, slides were mounted in 50% glycerol in PBS. For wholemount staining,
532 samples were washed in 0.3% PBTr and blocked in 1% BSA (Merck), 0.3% PBTr for at least
533 2 h. The samples were then incubated with primary antibodies in the blocking solution

overnight at 4°C. On the second day, the samples were washed at least five times in 0.3% PBTr and then incubated with secondary antibodies and DAPI (Invitrogen) diluted in PBS overnight at 4°C. The samples were then washed with PBS at least five times the next day and mounted in 50% glycerol in PBS. The following primary antibodies were used: Dylight 549 Mab (Hypoxyprobe-1 Inc, 1:200) antibody to detect hypoxyprobe labelling, HIF-1α (1:100, Novus Biologicals), HIF-2α (1:100, R&D Systems), endomucin (1:50, Santa Cruz Biotech), podoplanin (1:200, Fitzgerald), WT1 (1:100, Abcam), Alexa Fluor™ 488 Phalloidin (1:250, ThermoFischer), actin alpha-smooth muscle Cy3 (1:100, Sigma), Anti-α-Actinin (Sarcomeric) (1:500, Sigma-Aldrich), CD31 (1:100, Abcam), smooth muscle Myosin heavy chain 11 (SM-MHC, 1:100, Abcam), SM22 alpha (1:100, Abcam).

RNA isolation and qRT-PCR analysis

Total RNA was isolated from frozen ventricles with Trizol (Invitrogen) using a teflon homogeniser followed by aspiration with a sterile 25-gauge needle and syringe (BD sciences). RNA was transcribed into cDNA utilizing random primers (Promega) with Superscript Reverse Transcriptase III (Life Technologies). Real-time quantitative PCR was performed on a ViiA™ 7 Real-Time PCR System (Applied Biosystems), using SYBR Green mix (Invitrogen). Gene expression was evaluated as DeltaCt relative to control (*Atp5b* and *Sdha*).

Heart dissociation and FACS sorting

Hearts from P1 and P7 mice were harvested and minced into a single cell suspension of FACS sorted live cells. Briefly, for each sample, 3 hearts collected from the same litter were pooled together and finely minced with a scalpel. Tissue was then digested by gentle agitation (180 rpm shaker) in Collagenase II (Gibco,) using a solution of 500 units/ml in HBSS at 37 °C for 45 minutes (P7 hearts) or 20 minutes (P1 hearts). Cell solutions were

560 then passed through a 70 µm filter, washed and incubated in Red Blood Cell lysis buffer
561 (Cell Signaling Technology) for 10 minutes at RT to remove red blood cells. Finally, isolated
562 single cardiac cells were centrifuged, resuspended in 2% FBS in PBS, passed through the
563 filtering cap of the FACS tubes and incubated with 1% 7-AAD viability stain (Invitrogen) for
564 10 minutes. Approximately $1x10^5$ live cells per sample were sorted using the BD FACSAria
565 Fusion Sorter.
566
567 *Single cell RNA-Sequencing*
568 FACS sorted cardiac cells viability and concentration were assessed by using an automated
569 cell counter and $1.5x10^4$ cells per sample were loaded onto the 10X Chromium system (10X
570 Genomics) to obtain a target cell recovery of ~6000 cells. Single cell RNA-seq libraries were
571 generated using Single Cell 3 Prime Reagent Kits v1.3 (10x Genomics) according to the
572 manufacturer's protocol. Sequencing was performed on an Illumina NovaSeq 6000 System
573 operated by the Oxford Genomics Centre at the Wellcome Centre for Human Genetics. Raw
574 sequence reads were aligned against the mouse mm10/GRCm38 reference transcriptome
575 using the Cell Ranger 3.1.0 pipeline (10x Genomics) and processed further using the
576 scRNA-seq analysis R package Seurat (v.3.2.3). Initial filtering removed cells expressing
577 less than 200 genes and genes that were expressed in less than 3 cells. To exclude low
578 quality cells and doublets we filtered out cells with a very high mitochondrial genes content
579 and cells that expressed more than 8000 genes. Based on these criteria, 19211 genes
580 across 5308 and 8734 cells for P1 and P7 samples respectively remained for downstream
581 analysis. Data from the two samples were combined and scaled by regressing out the
582 nUMIs, percentage of mitochondrial gene expression and cell cycle. To correct for batch
583 effect, samples were integrated using the Harmony package (v.1.0). Uniform manifold
584 approximation and projection (UMAP) was performed on the scRNAseq harmonised cell
585 embeddings and unbiased clustering was obtained using the FindCluster function of the

586 Seurat pipeline. Cluster cell types were annotated using a combination of differentially
587 expressed markers, identified using the Seurat FindAllMarkers function and the expression
588 of selected canonical markers for specific cell types. The Epicardial cell cluster was then
589 identified and subsetted into a new Seurat object with raw reads counts. The standard
590 Seurat pipeline described above was performed and the Model-based Analysis of Single-
591 cell Transcriptomics test (MAST v.1.14.0) was used to analyse the differential gene
592 expression between the P1 and P7 groups in the epicardial cells. Finally, differentially
593 expressed genes were ranked based on both the fold change and p value (avg_logFC * -
594 log10 of the p_val) and the ranked list was submitted to the Metascape platform
595 (www.metascape.org) to identify enriched pathways in the P1 or P7 group, respectively.
596
597 *Cardiac cine-MRI*
598 Cardiac cine-MRI was performed at 7T using a Varian DDR system. Briefly, mice were
599 anaesthetised with 2% isoflurane in O2, and positioned supine in a custom animal handling
600 system with homeothermic control. Prospectively gated proton cardiac images were
601 acquired with a partial Fourier accelerated spoiled gradient echo CINE sequence (TR 5.9
602 ms, TE 2.2 ms, 30 kHz bandwidth, 25º FA, approximately 20-30 frames gated to the R wave
603 with a 4 ms postlabel delay; 20% partial acquisition; 4 averages) with a 72 mm volume
604 transmit/4 channel surface receive coil (Rapid Biomedical GmbH) in order to acquire two
605 and four chamber long-axis views and a short axis stack for functional quantification
606 (128x128 matrix; 25.6 mm^2 FOV; 0.7 mm slice thickness, 0.2 mm resolution in-plane). Non-
607 acquired partial Fourier data was reconstructed via the method of projection onto convex
608 sets prior to a simple, cartesian, DFT. Blinded image analysis was performed in ImageJ as
609 described previously[66].
610
611 *Image Analysis*

612 For quantification of immunofluorescence of cryosections, images were captured on an
613 Olympus FluoView 3000 confocal microscope and analysed with Fiji (NIH) and AngioTool[67].
614 To quantify nuclear fluorescence, a macro was written to identify all DAPI-stained nuclei and
615 to analyse nuclear fluorescence based on the DAPI mask. To localise WT1+ cells in the
616 epicardium and myocardium, cells were manually counted.
617
618 *Statistical Analysis*
619 All data are presented as mean ± standard error of the mean (SEM) or as median, inter-
620 quartile range (IQR) and upper and lower limits. Statistical analysis was performed on
621 GraphPad Prism 8 software. The statistical significance between two groups was
622 determined using an unpaired two-tailed Student's t-test, these included an F-test to confirm
623 the two groups had equal variances. Among three or more groups, one-way analysis of
624 variance (ANOVA) followed up by Dunnett's or Tukey's multiple comparison tests were
625 used. A value of $p \leq 0.05$ was considered statistically significant.
626

Acknowledgements

We are very grateful to Prof. Peter J Ratcliffe for technical advice and highly informative scientific discussions throughout the project. We would like to thank Biomedical Services Unit for animal husbandry and Micron Oxford Advanced Bioimaging Unit (supported by Wellcome Strategic Awards 091911/B/10/Z and 107457/Z/15/Z) for access to and training in the use of confocal microscopy. This work was funded by the British Heart Foundation (BHF chair award to PRR: CH/11/1/28798; BHF programme grant to PRR: RG/18/33532; BHF Intermediate Basic Science Research Fellowship to JMV: FS/19/31/34158) and supported by the BHF Oxbridge Regenerative Medicine Centre (RM/17/2/33380).

Author Contributions

PRR conceived the original project and sourced funding. PRR and JMV oversaw the project direction and data analyses. EG and ELP carried out experiments and analysed the data. CDV and MGR preformed surgeries. DP carried out the scRNA-seq experiment and bioinformatic analyses. RPC supervised the scRNA-Seq experiment and computational analyses. RS and DRM, assisted with the analysis of HIF-1β ChIP-seq datasets. TB and CWP provided *Rosa*$^{26+/CreERT2}$*;Hif1a*$^{fl/fl}$ and *Rosa*$^{26+/CreERT2}$*;Phd2*$^{fl/fl}$ mouse strains, and provided advice and technical assistance. CAC performed blinded MRI scanning and analyses. EG wrote the main draft of the manuscript. PRR and JMV contributed to editing of the final manuscript.

Competing interests

The authors declare no competing interests.

653 **References**

654 1. Simões, F. C. & Riley, P. R. The ontogeny, activation and function of the epicardium
655 during heart development and regeneration. *Dev.* **145**, (2018).
656 2. Martínez-Estrada, O. M. *et al.* Wt1 is required for cardiovascular progenitor cell
657 formation through transcriptional control of Snail and E-cadherin. *Nat. Genet.* **42**,
658 89–93 (2010).
659 3. Li, P. *et al.* IGF signaling directs ventricular cardiomyocyte proliferation during
660 embryonic heart development. *Development* **138**, 1795–1805 (2011).
661 4. von Gise, A. *et al.* WT1 regulates epicardial epithelial to mesenchymal transition
662 through β-catenin and retinoic acid signaling pathways. *Dev Biol* **356**, 421–431
663 (2011).
664 5. Gittenberger-de Groot, A. C., Vrancken Peeters, M. P. F. M., Mentink, M. M. T.,
665 Gourdie, R. G. & Poelmann, R. E. Epicardium-derived cells contribute a novel
666 population to the myocardial wall and the atrioventricular cushions. *Circ. Res.* **82**,
667 1043–1052 (1998).
668 6. Mikawa, T. & Gourdie, R. G. Pericardial mesoderm generates a population of
669 coronary smooth muscle cells migrating into the heart along with ingrowth of the
670 epicardial organ. *Dev. Biol.* **174**, 221–232 (1996).
671 7. Katz, T. C. *et al.* Distinct Compartments of the Proepicardial Organ Give Rise to
672 Coronary Vascular Endothelial Cells. *Dev. Cell* **22**, 639–650 (2012).
673 8. Smart, N. *et al.* De novo cardiomyocytes from within the activated adult heart after
674 injury. *Nature* **474**, 640–644 (2011).
675 9. Vieira, J. M. *et al.* BRG1-SWI/SNF-dependent regulation of the Wt1 transcriptional
676 landscape mediates epicardial activity during heart development and disease. *Nat.*
677 *Commun.* **8**, (2017).
678 10. Zhou, B. & Pu, W. T. Epicardial epithelial-to-mesenchymal transition in injured heart.

679 *J. Cell. Mol. Med.* **15**, 2781–2783 (2011).
680 11. Price, E. L., Vieira, J. M. & Riley, P. R. Model organisms at the heart of regeneration.
681 *DMM Dis. Model. Mech.* **12**, (2019).
682 12. Porrello, E. R. & Olson, E. N. A neonatal blueprint for regeneration. *Stem Cell Res.*
683 **13**, 556–570 (2014).
684 13. Porrello, E. R. *et al.* Transient Regenerative Potential of the Neonatal Mouse Heart
685 Enzo. *Science (80-.).* **331**, 1078–1080 (2011).
686 14. Haubner, B. J. *et al.* Functional Recovery of a Human Neonatal Heart after Severe
687 Myocardial Infarction. *Circ. Res.* **118**, 216–221 (2016).
688 15. Wang, J., Cao, J., Dickson, A. L. & Poss, K. D. Epicardial regeneration is guided by
689 cardiac outflow tract and Hedgehog signalling. *Nature* **522**, (2015).
690 16. Zhou, B. *et al.* Adult mouse epicardium modulates myocardial injury by secreting
691 paracrine factors. *J Clin Invest* **121**, 1894–1904 (2011).
692 17. Smart, N. *et al.* Thymosin β4 facilitates epicardial neovascularization of the injured
693 adult heart. *Ann. N. Y. Acad. Sci.* **1194**, 97–104 (2010).
694 18. van Wijk, B., Gunst, Q. D., Moorman, A. F. M. & van den Hoff, M. J. B. Cardiac
695 Regeneration from Activated Epicardium. *PLoS One* **7**, (2012).
696 19. Puente, B. N. *et al.* The oxygen-rich postnatal environment induces cardiomyocyte
697 cell-cycle arrest through DNA damage response. *Cell* **157**, 565–579 (2014).
698 20. Kimura, W. *et al.* Hypoxia fate mapping identifies cycling cardiomyocytes in the adult
699 heart. *Nature* **523**, (2015).
700 21. Nakada, Y. *et al.* Hypoxia induces heart regeneration in adult mice. *Nature* **541**,
701 (2017).
702 22. Kaelin, W. G. & Ratcliffe, P. J. Oxygen Sensing by Metazoans: The Central Role of
703 the HIF Hydroxylase Pathway. *Mol. Cell* **30**, 393–402 (2008).
704 23. Semenza, G. L. & Wang, G. L. A nuclear factor induced by hypoxia via de novo

protein synthesis binds to the human erythropoietin gene enhancer at a site required for transcriptional activation. *Mol. Cell. Biol.* **12**, 5447–5454 (1992).

24. Maxwell, P. H. *et al.* The tumour suppressor protein VHL targets hypoxia-inducible factors for oxygen-dependent proteolysis. *Nature* **399**, 271–275 (1999).

25. Forsythe, J. A. *et al.* Activation of vascular endothelial growth factor gene transcription by hypoxia-inducible factor 1. *Mol. Cell. Biol.* **16**, 4604–4613 (1996).

26. Ebert, B. L., Firth, J. D. & Ratcliffe, P. J. Hypoxia and mitochondrial inhibitors regulate expression of glucose transporter-1 via distinct cis-acting sequences. *J. Biol. Chem.* **270**, 29083–29089 (1995).

27. Hu, C.-J., Wang, L.-Y., Chodosh, L. A., Keith, B. & Simon, M. C. Differential Roles of Hypoxia-Inducible Factor 1α (HIF-1α) and HIF-2α in Hypoxic Gene Regulation. *Molecular and Cellular Biology* vol. 23 9361–9374 (2003).

28. Schödel, J. *et al.* High-resolution genome-wide mapping of HIF-binding sites by ChIP-seq. *Blood* **117**, 207–217 (2011).

29. Dunwoodie, S. L. The Role of Hypoxia in Development of the Mammalian Embryo. *Dev. Cell* **17**, 755–773 (2009).

30. Jain, S., Maltepe, E., Lu, M. M., Simon, C. & Bradfield, C. A. Expression of ARNT, ARNT2, HIF1α, HIF2α and Ah receptor mRNAs in the developing mouse. *Mech. Dev.* **73**, 117–123 (1998).

31. Compernolle, V. *et al.* Cardia bifida, defective heart development and abnormal neural crest migration in embryos lacking hypoxia-inducible factor-1α. *Cardiovasc. Res.* **60**, 569–579 (2003).

32. Krishnan, J. *et al.* Essential role of developmentally activated hypoxia-inducible factor la for cardiac morphogenesis and function. *Circ. Res.* **103**, 1139–1146 (2008).

33. Ryan, H. E., Lo, J. & Johnson, R. S. HIF-1 alpha is required for solid tumor formation and embryonic vascularization. *EMBO J* **17**, 3005–3015 (1998).

731 34. Peng, J., Zhang, L., Drysdale, L. & Fong, G.-H. The transcription factor EPAS-1
732 hypoxia-inducible factor 2α plays an important role in vascular remodeling.pdf. *Proc*
733 *Natl Acad Sci USA* **97**, 8386–91 (2000).
734 35. Tian, H., Hammer, R. E., Matsumoto, A. M., Russell, D. W. & McKnight, S. L. The
735 hypoxia-responsive transcription factor EPAS1 is essential for catecholamine
736 homeostasis and protection against heart failure during embryonic development.
737 *Genes Dev.* **12**, 3320–3324 (1998).
738 36. Adelman, D. M., Gertsenstein, M., Nagy, A., Simon, M. C. & Maltepe, E. Placental
739 cell fates are regulated in vivo by HIF-mediated hypoxia responses. *Genes Dev.* **14**,
740 3191–3203 (2000).
741 37. Takeda, K. *et al.* Placental but Not Heart Defects Are Associated with Elevated
742 Hypoxia-Inducible Factor α Levels in Mice Lacking Prolyl Hydroxylase Domain
743 Protein 2. *Mol. Cell. Biol.* **26**, 8336–8346 (2006).
744 38. Tao, J., Doughman, Y., Yang, K., Ramirez-Bergeron, D. & Watanabe, M. Epicardial
745 HIF signaling regulates vascular precursor cell invasion into the myocardium. *Dev*
746 *Biol* **376**, 136–149 (2013).
747 39. Tao, J., Barnett, J., Watanabe, M. & Ramírez-Bergeron, D. Hypoxia Supports
748 Epicardial Cell Differentiation in Vascular Smooth Muscle Cells through the
749 Activation of the TGFβ Pathway. *J. Cardiovasc. Dev. Dis.* **5**, 19 (2018).
750 40. Wagner, K.-D. *et al.* Oxygen-regulated expression of the Wilms' tumor suppressor
751 Wt1 involves hypoxia-inducible factor-1 (HIF-1). *FASEB J* **17**, 1364–1366 (2003).
752 41. Krueger, K., Catanese, L., Sciesielski, L. K., Kirschner, K. M. & Scholz, H. Deletion
753 of an intronic HIF-2α binding site suppresses hypoxia-induced WT1 expression.
754 *Biochimica et Biophysica Acta - Gene Regulatory Mechanisms* vol. 1862 71–83
755 (2019).
756 42. Macdougall, I. C., Akizawa, T., Berns, J. S., Bernhardt, T. & Krueger, T. Effects of

molidustat in the treatment of anemia in CKD. *Clin. J. Am. Soc. Nephrol.* **14**, (2019).

43. Henry, D. H. *et al.* Roxadustat (FG4592; ASP1517; AZD9941) in the Treatment of Anemia in Patients with Lower Risk Myelodysplastic Syndrome (LR-MDS) and Low Red Blood Cell (RBC) Transfusion Burden (LTB). *Blood* **134**, (2019).
44. Chen, N. *et al.* Roxadustat for Anemia in Patients with Kidney Disease Not Receiving Dialysis. *N. Engl. J. Med.* **381**, (2019).
45. Chen, N. *et al.* Roxadustat Treatment for Anemia in Patients Undergoing Long-Term Dialysis. *N. Engl. J. Med.* **381**, (2019).
46. Raleigh, J. A., Chou, S. C., Arteel, G. E. & Horsman, M. R. Comparisons among pimonidazole binding, oxygen electrode measurements, and radiation response in C3H mouse tumors. *Radiat. Res.* **151**, (1999).
47. Zhou, B. *et al.* Epicardial progenitors contribute to the cardiomyocyte lineage in the developing heart. *Nature* **454**, (2008).
48. Moore, A. W., McInnes, L., Kreidberg, J., Hastie, N. D. & Schedl, A. YAC complementation shows a requirement for Wt1 in the development of epicardium, adrenal gland and throughout nephrogenesis. *Development* **126**, (1999).
49. Smythies, J. A. *et al.* Inherent DNA -binding specificities of the HIF -1α and HIF -2α transcription factors in chromatin . *EMBO Rep.* **20**, (2019).
50. Somsuan, K. *et al.* ARID1A knockdown triggers epithelial-mesenchymal transition and carcinogenesis features of renal cells: Role in renal cell carcinoma. *FASEB J.* **33**, (2019).
51. Bochmann, L. *et al.* Revealing new mouse epicardial cell markers through transcriptomics. *PLoS One* **5**, (2010).
52. Cui, M. *et al.* Dynamic Transcriptional Responses to Injury of Regenerative and Non-regenerative Cardiomyocytes Revealed by Single-Nucleus RNA Sequencing. *Dev. Cell* **53**, (2020).

53. Lepilina, A. *et al.* A Dynamic Epicardial Injury Response Supports Progenitor Cell Activity during Zebrafish Heart Regeneration. *Cell* **127**, (2006).
54. Duim, S. N., Kurakula, K., Goumans, M. J. & Kruithof, B. P. T. Cardiac endothelial cells express Wilms' tumor-1. Wt1 expression in the developing, adult and infarcted heart. *J. Mol. Cell. Cardiol.* **81**, (2015).
55. Chen, H. I. *et al.* The sinus venosus contributes to coronary vasculature through VEGFC-stimulated angiogenesis. *Dev.* **141**, (2014).
56. Tian, X. *et al.* Subepicardial endothelial cells invade the embryonic ventricle wall to form coronary arteries. *Cell Res.* **23**, (2013).
57. Scully, D. *et al.* Hypoxia promotes production of neural crest cells in the embryonic head. *Dev.* **143**, (2016).
58. Lupu, I. E., Redpath, A. N. & Smart, N. Spatiotemporal Analysis Reveals Overlap of Key Proepicardial Markers in the Developing Murine Heart. *Stem Cell Reports* **14**, (2020).
59. Liang, J. *et al.* Concise Review: Reduction of Adverse Cardiac Scarring Facilitates Pluripotent Stem Cell-Based Therapy for Myocardial Infarction. *Stem Cells* vol. 37 (2019).
60. Simões, F. C. *et al.* Macrophages directly contribute collagen to scar formation during zebrafish heart regeneration and mouse heart repair. *Nat. Commun.* **11**, (2020).
61. Koth, J. *et al.* Runx1 promotes scar deposition and inhibits myocardial proliferation and survival during zebrafish heart regeneration. *Dev.* **147**, (2020).
62. Higgins, D. F. *et al.* Hypoxic induction of Ctgf is directly mediated by Hif-1. *Am. J. Physiol. - Ren. Physiol.* **287**, (2004).
63. Pitulescu, M. E., Schmidt, I., Benedito, R. & Adams, R. H. Inducible gene targeting in the neonatal vasculature and analysis of retinal angiogenesis in mice. *Nature*

Protocols vol. 5 (2010).

64. De Villiers, C. & Riley, P. R. A Refined Protocol for Coronary Artery Ligation in the Neonatal Mouse. *Curr. Protoc.* **1**, (2021).

65. Chen, T. H. P. *et al.* Epicardial induction of fetal cardiomyocyte proliferation via a retinoic acid-inducible trophic factor. *Dev. Biol.* **250**, (2002).

66. Carr, C. A. *et al.* Bone marrow-derived stromal cells home to and remain in the infarcted rat heart but fail to improve function: An in vivo cine-MRI study. *Am. J. Physiol. - Hear. Circ. Physiol.* **295**, (2008).

67. Zudaire, E., Gambardella, L., Kurcz, C. & Vermeren, S. A computational tool for quantitative analysis of vascular networks. *PLoS One* **6**, (2011).

820 **Figure Legends**

821

822 **Figure 1. The epicardium is hypoxic at later stages of heart development.**
823 Representative images of immunostaining for DAPI (blue), HP1 (red) and EMCN, WT1, HIF-
824 1α and HIF-2α (green) on cryosections of foetal hearts at E12.5 (a), E14.5 (b), E16.5 (c) and
825 E18.5 (d). Arrowheads indicate overlap between HP1 and WT1, HIF-1α or HIF-2α. n=6
826 hearts per stage. AV groove= atrioventricular groove, IVS= interventricular septum, RV=
827 right ventricle, LV= left ventricle. Whole heart scale bars, 200μm; high magnification scale
828 bars,100μm.

829

830 **Figure 2. Epicardial loss of *Hif1α* leads to reduced WT1 expression and impaired EMT.**
831 (a-b) Representative images of immunostaining for EMCN (green), WT1 (red), PDPN (white)
832 and DAPI (blue), on coronal sections of hearts from (a) *Hif1a*$^{fl/fl}$ (CTR) or (b)
833 *Wt1*$^{CreERT2/+}$;*Hif1a*$^{fl/fl}$ (KO) embryos at E16.5. Images on the right of each panel represent
834 high magnifications of boxed regions. Scale bars, 200μm. (c,d) Percentage of WT1+ cells
835 per section in (c) the epicardium or (d) the myocardium. (e) Muscle compaction index and
836 (f) fractal analysis used to determine the complexity of myocardial trabeculae. n=3-4
837 hearts/group. (g) Whole-mount immunostaining for EMCN (green) to visualize coronary
838 vasculature from CTR and KO embryos at E16.5. Scale bars, 500μm. IVS= interventricular
839 septum, RV= right ventricle, LV= left ventricle. (h-j) Quantification of the coronary
840 vasculature as (h) total vessel length, (i) number of junctions and (j) end points. n = 3
841 hearts/group. Data presented as median, inter-quartile range (IQR) and upper and lower
842 limits. Data analysed by student t-test, *$p<0.05$.

843

844 **Figure 3. Stabilisation of HIF signalling promotes Wt1 expression and enhances**
845 **epicardial EMT.** (a,b) Representative images of immunostaining for α smooth muscle actin

(α-SMA, red), WT1 (red) and DAPI nuclear stain (blue) and (c) quantification of nuclear intensity of WT1 signal on epicardial explants derived from *Phd2*$^{fl/fl}$ (CTR) and *Rosa26*$^{+/CreERT2}$;*Phd2*$^{fl/fl}$ (KO) embryos at E11.5. n=3/group. (d-f) Representative images of immunostaining for Phalloidin (green), α-SMA (red), WT1 (red) and DAPI nuclear stain (blue), and (g) quantification of nuclear intensity of WT1 signal on epicardial explants derived from wild type embryos at E11.5 treated with DMSO (Control), Roxadustat (FG-4592) or Molidustat (BAY 85-3934). n= 5-6/group. Scale bars, 50μm. Arrowheads indicate stress fibres. Data presented as median, inter-quartile range (IQR) and upper and lower limits. Data analysed by student t-test and one-way ANOVA with Dunnett's post-hoc test, *p<0.05.

Figure 4. HIF signalling is downregulated in between P1 and P7 in neonatal mice. (a) UMAP representation of different cell populations in the neonatal heart at postnatal day (P) 1 and P7. (b) Stacked violin plots showing expression of canonical Epi-enriched genes *Upk3b*, *Upk1b*, *Bnc*, *Dmkn*. (c) Heatmap showing biological processes enriched in the Epi cluster at P1 and P7. Violin plots showing expression of HIF target genes (d) *Vegfa* and *Pdk3*, and (e) *Phd2* at P1 and P7. (f) Real time RT-PCR analysis of *Phd2*, n=4 mice per group. (g) Representative images of immunostaining for WT1 (green), ACTN2 (red), PDPN (white) and DAPI nuclear stain (blue) at P1 and P7. Images to the right are magnified views of boxed regions shown in whole heart images. Arrowheads indicate expression of WT1 in the epicardium. IVS= interventricular septum, RV= right ventricle, LV= left ventricle. Whole heart scale bars, 200μm; high magnification scale bars,100μm. n=3 hearts per stage. Data presented Mean ±SEM. Data analysed by one-way ANOVA with Tukey's post-hoc test **p<0.01; ****p<0.0001. Epi, epicardium.

Figure 5. Loss of *Phd2* induces WT1 epicardial expression and improves heart regeneration post-MI. (a) Representative images of immunostaining for WT1 (green),

ACTN2 (red), PDPN (white) and DAPI nuclear stain (blue) on transverse apical sections of hearts from *Phd2*$^{fl/fl}$ (CTR) and *Rosa26*$^{+/CreERT2}$;*Phd2*$^{fl/fl}$ (KO) mice and (b-e) quantification of number of WT1 positive cells at 4 days post-injury (dpi). Images on the right represent high magnification views of boxed regions shown in whole heart images. Arrowheads indicate expression of WT1 in the epicardium (determined by co-expression with PDPN); arrows indicate WT1 expression in non-epicardial cells. Epi, epicardium; myo, myocardium. Whole heart scale bars, 200μm; high magnification scale bars,100μm. n=4 hearts per group. Data presented as median, IQR and upper and lower limits. Data analysed by Student's t-test **p<0.01. (f) Representative images of immunostaining for CD31 (green), SM-MHC (red) and DAPI (blue) on transverse apical sections of hearts from CTR and KO hearts at 4dpi. Images in top right corner represent high magnifications of boxed region. n=4 hearts per group. RV= right ventricle, LV= left ventricle. Scale bars, 200μm, high magnification scale bars, 50μm. (g) Masson's Trichrome stained transverse sections to show cardiac fibrosis (blue) at 21dpi. * denotes suture placement. Scale bars, 1mm. n=3 for *Phd2*$^{fl/fl}$, n=1 for *Rosa26*$^{+/CreERT2}$;*Phd2*$^{fl/fl}$.

Figure 6. Pharmacological treatment with PHD inhibitors induces WT1 expression. (a) Representative images of immunostaining for WT1 (red), PDPN (white) and DAPI nuclear stain (blue) on sections of hearts from animals treated with either (a) saline (Control), (b) Roxadustat (FG-4592) or (c) Molidustat (BAY 85-3934) and (d-g) quantification of number of WT1 positive cells at 9 days post-injury (dpi). Images on the right represent high magnification views of boxed regions shown in whole heart images. Arrowheads indicate expression of WT1 in the epicardium (determined by co-expression with PDPN). Whole heart scale bars, 200μm; high magnification scale bars, 100μm. n=4 hearts per group. (h) Representative images of immunostaining for CD31 (green), α-SMA (red) and DAPI (blue) on sections of hearts from animals treated with either (h) saline (Control), (i) Roxadustat

(FG-4592) or (j) Molidustat (BAY 85-3934) and (k) quantification of number of vessels at 9 dpi. n=3 hearts per group. IVS= interventricular septum, RV= right ventricle, LV= left ventricle. Scale bars 200μm, high magnification scale bars, 50μm. Data presented as median, IQR and upper and lower limits. Data analysed by one-way ANOVA with Dunnett's post-hoc test *p<0.05.

Figure 7. Pharmacological stabilisation of HIF induces new coronary vessel formation and improves heart function. Representative images of immunostaining for α-smooth muscle actin (α-SMA, red), CD31 (green) and DAPI nuclear stain (blue) on sections of hearts from animals treated with either (a) saline (Control), (b) Roxadustat (FG-4592) or (c) Molidustat (BAY 85-3934) and (d) quantification of number of new vessels at 9 days post-injury (dpi). Images below represent high magnification views of boxed regions shown in whole heart images. Arrowheads indicate vessel (determined by co-expression of CD31 and α-SMA). Whole heart scale bars, 200μm; high magnification scale bars,100μm. n=3-4 hearts per group. (e) Representative mid-ventricular short-axis MRI frames for control, Roxadustat and Molidustat treated heart. (f-h) MRI analyses of infarcted control and treated hearts at 21 dpi showing reduced CO (f), SV (g), and EDV (h) in Molidustat treated animals, compared with controls. n=5-7 hearts per group. (i) Representative images and (j) quantification of Masson's Trichrome stained transverse sections to show cardiac fibrosis (blue) at 21dpi. * denotes suture placement. Scale bars, 1mm. Data presented as median, IQR and upper and lower limits. Data analysed by one-way ANOVA with Dunnett's post-hoc test *p<0.05, **p<0.01.

Figures

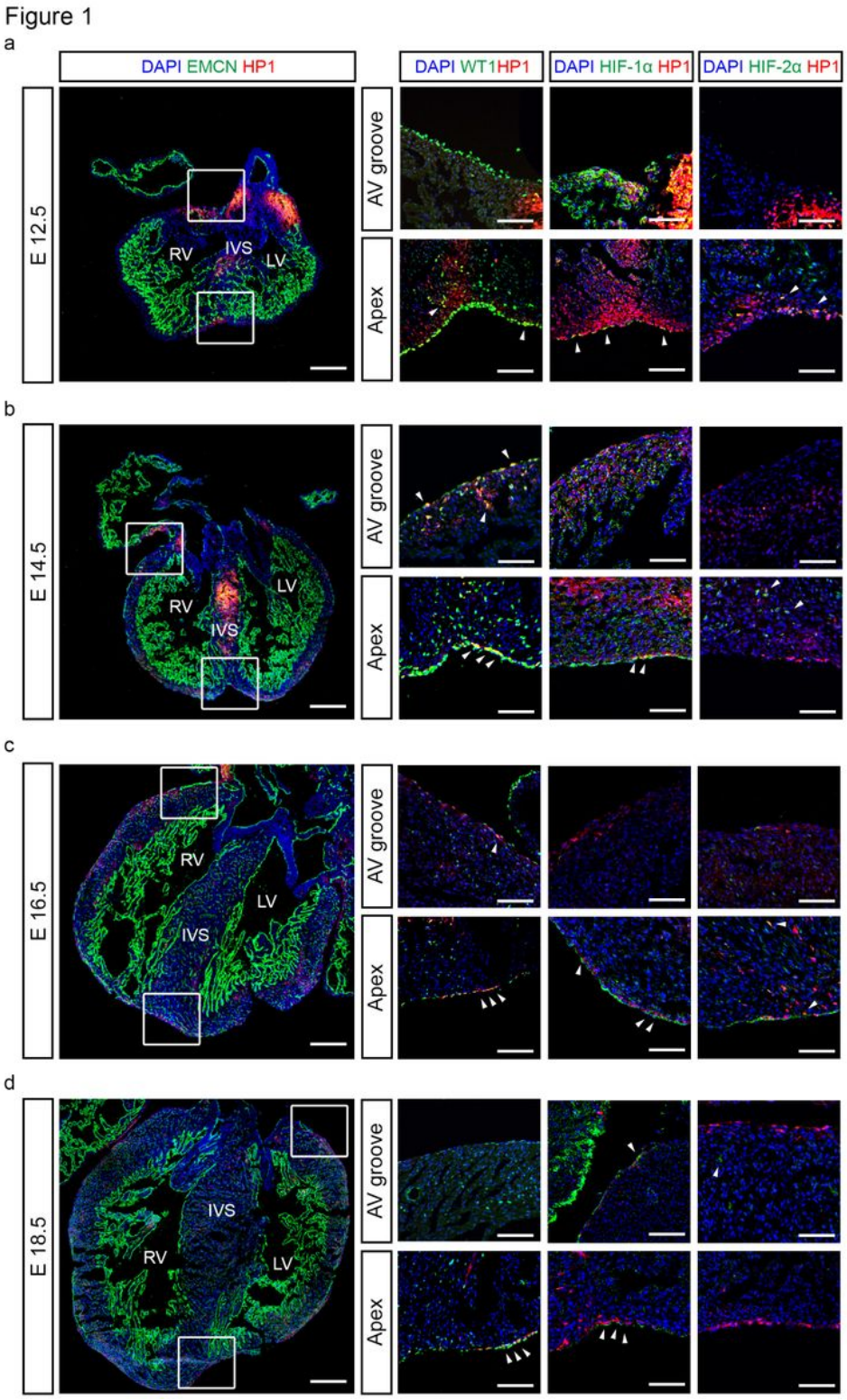

Figure 1

The epicardium is hypoxic at later stages of heart development. Representative images of immunostaining for DAPI (blue), HP1 (red) and EMCN, WT1, HIF- 1α and HIF-2α (green) on cryosections of foetal hearts at E12.5 (a), E14.5 (b), E16.5 (c) and E18.5 (d). Arrowheads indicate overlap between HP1

and WT1, HIF-1α or HIF-2α. n=6hearts per stage. AV groove= atrioventricular groove, IVS= interventricular septum, RV= right ventricle, LV= left ventricle. Whole heart scale bars, 200μm; high magnification scale bars,100μm.

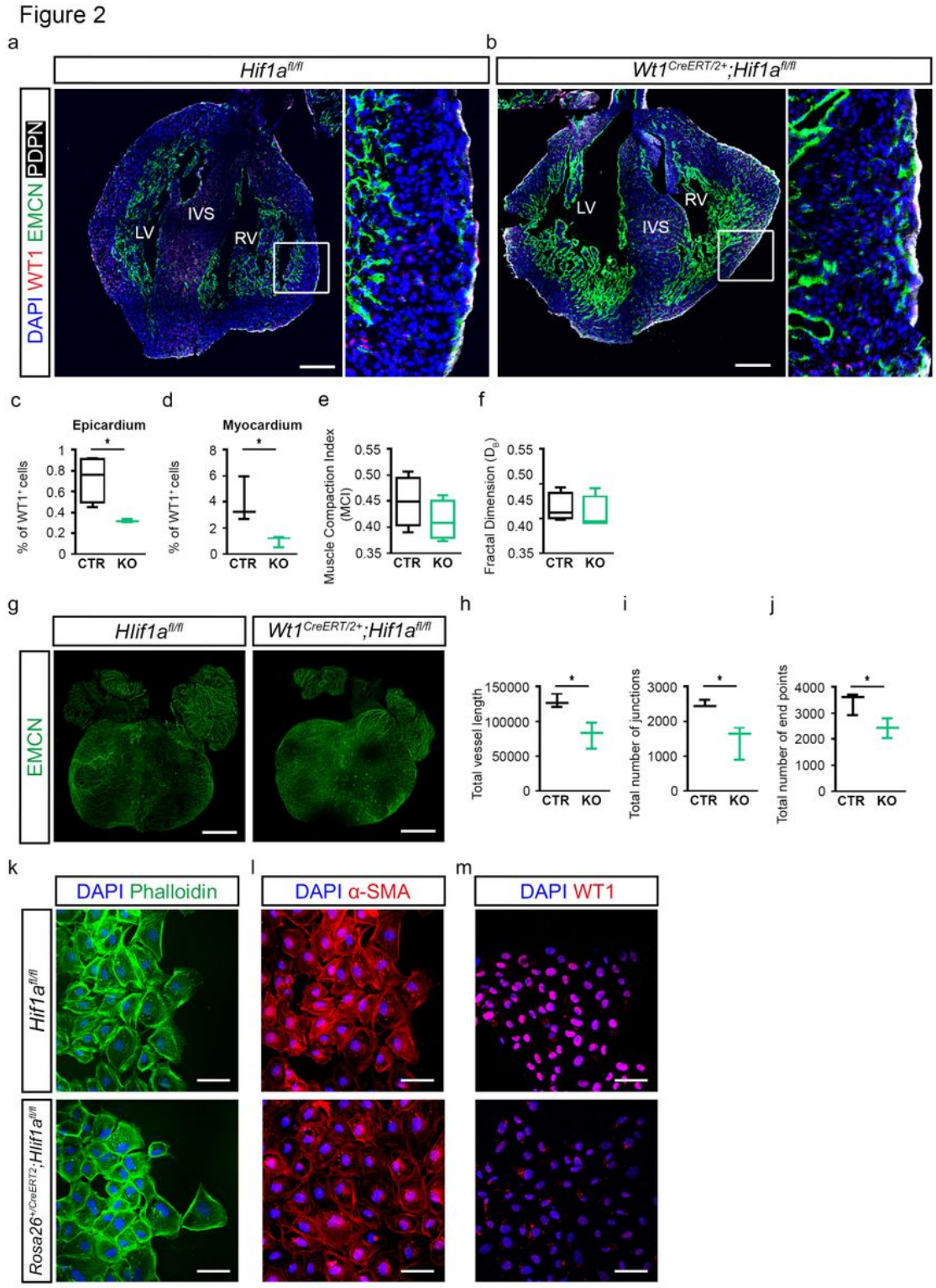

Figure 2

Epicardial loss of Hif1α leads to reduced WT1 expression and impaired EMT. (a-b) Representative images of immunostaining for EMCN (green), WT1 (red), PDPN (white) and DAPI (blue), on coronal sections of

hearts from (a) Hif1afl/fl (CTR) or (b) Wt1CreERT2/+;Hif1afl/fl (KO) embryos at E16.5. Images on the right of each panel represent high magnifications of boxed regions. Scale bars, 200μm. (c,d) Percentage of WT1+ cells per section in (c) the epicardium or (d) the myocardium. (e) Muscle compaction index and (f) fractal analysis used to determine the complexity of myocardial trabeculae. n=3-4 hearts/group. (g) Whole-mount immunostaining for EMCN (green) to visualize coronary vasculature from CTR and KO embryos at E16.5. Scale bars, 500μm. IVS= interventricular septum, RV= right ventricle, LV= left ventricle. (h-j) Quantification of the coronary 839 vasculature as (h) total vessel length, (i) number of junctions and (j) end points. n = 3 hearts/group. Data presented as median, inter-quartile range (IQR) and upper and lower limits. Data analysed by student t-test, *$p<0.05$.

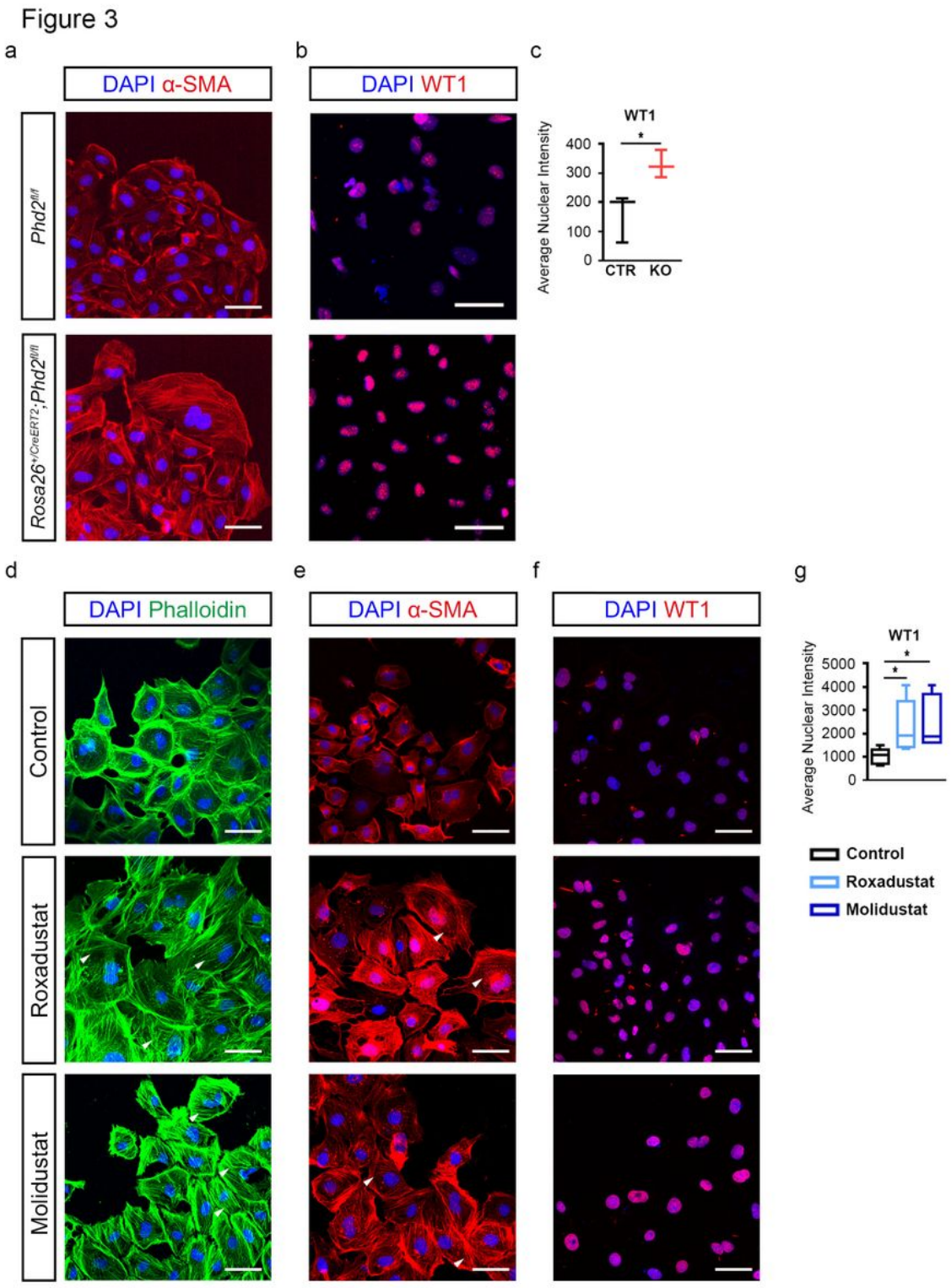

Figure 3

Stabilisation of HIF signalling promotes Wt1 expression and enhances epicardial EMT. (a,b) Representative images of immunostaining for α smooth muscle actin (α-SMA, red), WT1 (red) and DAPI nuclear stain (blue) and (c) quantification of nuclear intensity of WT1 signal on epicardial explants derived from Phd2fl/fl (CTR) and Rosa26+/CreERT2;Phd2fl/fl (KO) embryos at E11.5. n=3/group. (d-f) Representative images of immunostaining for Phalloidin (green), α-SMA (red), WT1 (red) and DAPI

nuclear stain (blue), and (g) quantification of nuclear intensity of WT1 signal on epicardial explants derived from wild type embryos at E11.5 treated with DMSO (Control), Roxadustat (FG-4592) or Molidustat (BAY 85-3934). n= 5-6/group. Scale bars, 50μm. Arrowheads indicate stress fibres. Data presented as median, inter-quartile range (IQR) and upper and lower limits. Data analysed by student t-test and one-way ANOVA with Dunnett's post-hoc test, *p<0.05.

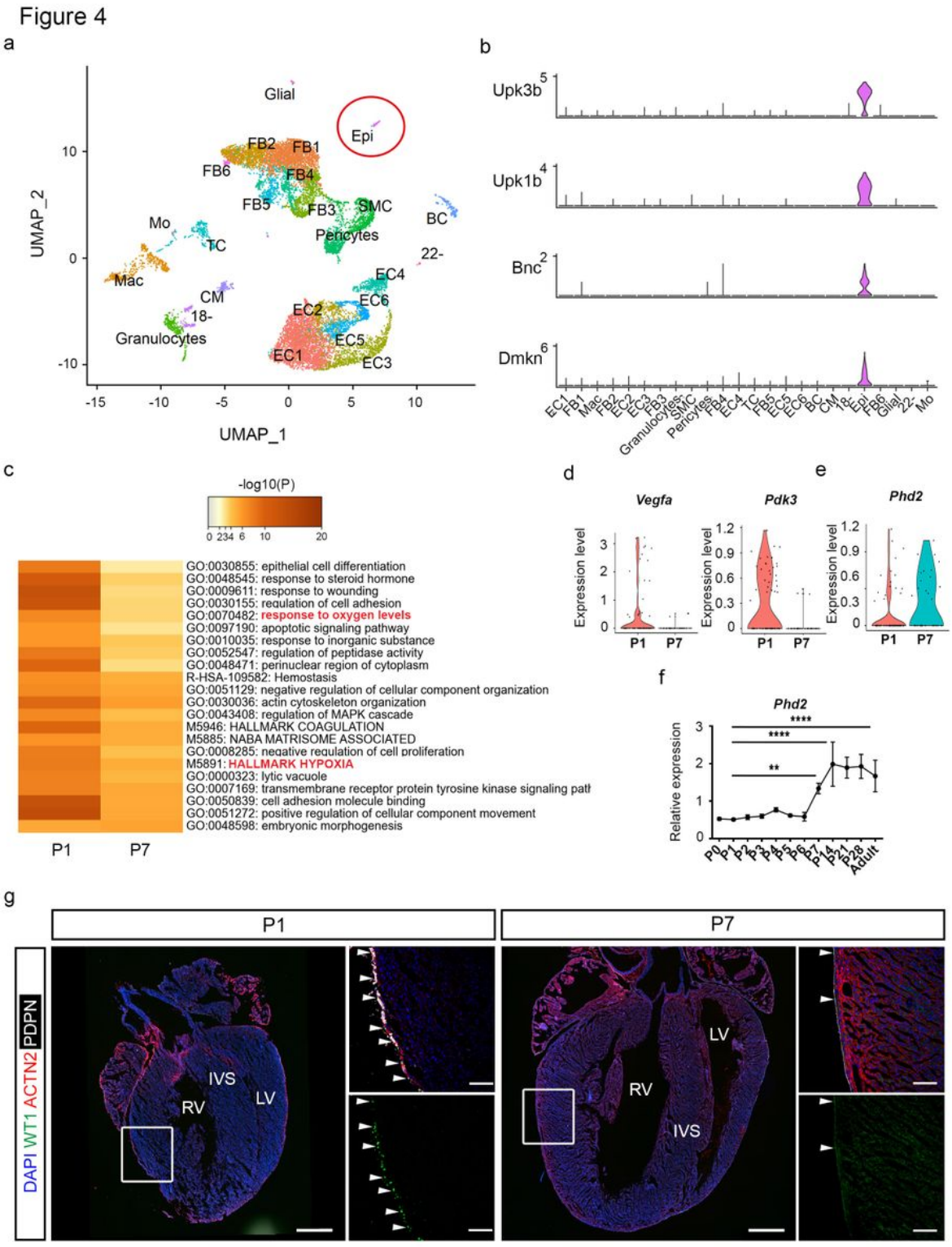

Figure 4

HIF signalling is downregulated in between P1 and P7 in neonatal mice. (a) 856 UMAP representation of different cell populations in the neonatal heart at postnatal day (P) 1 and P7. (b) Stacked violin plots showing expression of canonical Epi-enriched genes Upk3b, Upk1b, Bnc, Dmkn. (c) Heatmap showing biological processes enriched in the Epi cluster at P1 and P7. Violin plots showing expression of HIF target genes (d) Vegfa and Pdk3, and (e) Phd2 at P1 and P7. (f) Real time RT-PCR analysis of Phd2, n=4 mice per group. (g) Representative images of immunostaining for WT1 (green), ACTN2 (red), PDPN (white) and DAPI nuclear stain (blue) at P1 and P7. Images to the right are magnified views of boxed regions shown in whole heart images. Arrowheads indicate expression of WT1 in the epicardium. IVS= interventricular septum, RV= right ventricle, LV= left ventricle. Whole heart scale bars, 200μm; high magnification scale bars,100μm. n=3 hearts per stage. Data presented Mean ±SEM. Data analysed by one-way ANOVA with Tukey's post-hoc test **p<0.01; ****p<0.0001. Epi, epicardium.

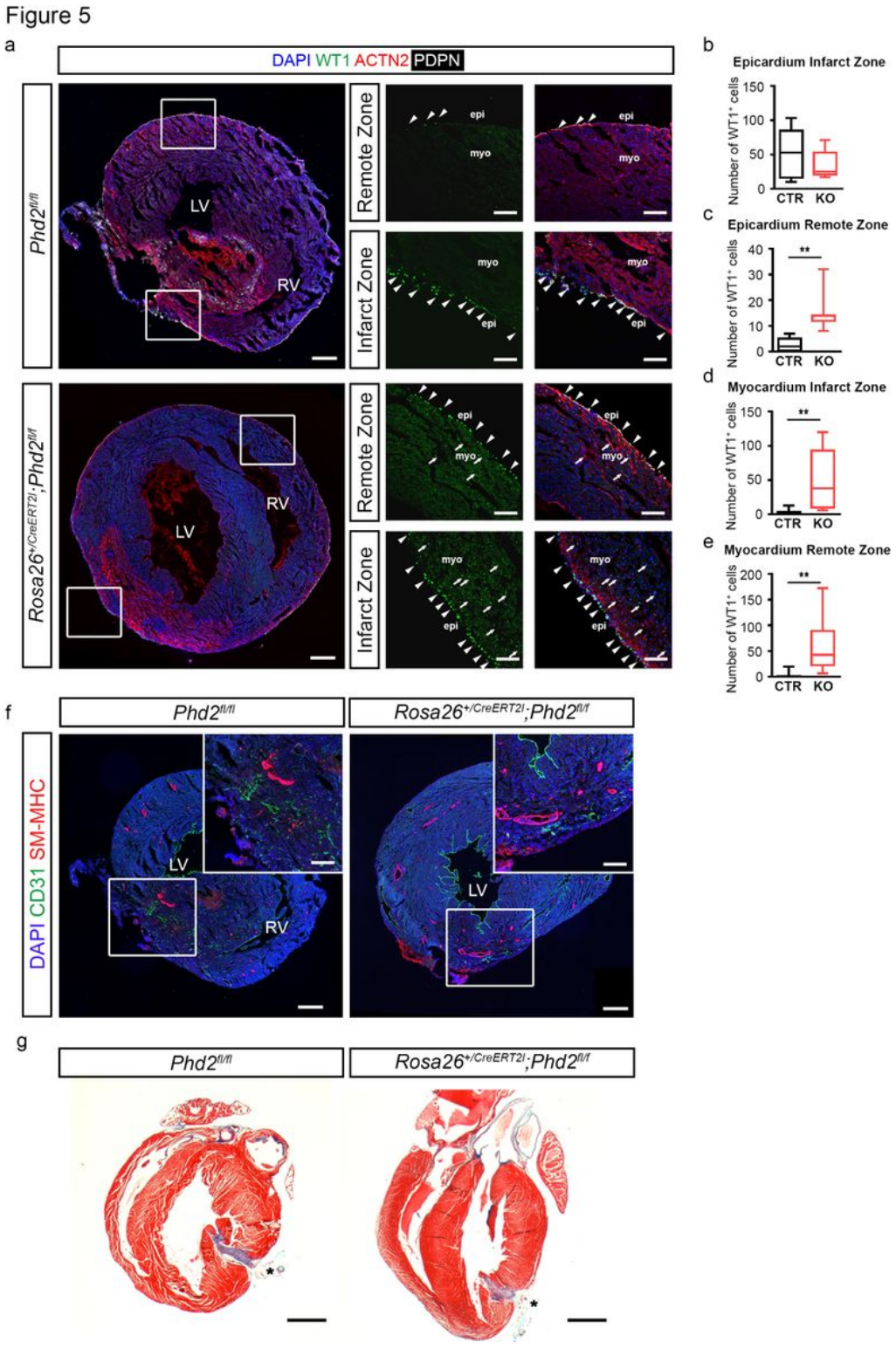

Figure 5

Loss of Phd2 induces WT1 epicardial expression and improves heart regeneration post-MI. (a) Representative images of immunostaining for WT1 (green), ACTN2 (red), PDPN (white) and DAPI nuclear stain (blue) on transverse apical sections of hearts from Phd2fl/fl (CTR) and Rosa26+/CreERT2;Phd2fl/fl (KO) mice and (b-e) quantification of number of WT1 positive cells at 4 days post-injury (dpi). Images on the right represent high magnification views of boxed regions shown in whole heart images. Arrowheads

indicate expression of WT1 in the epicardium (determined by co-expression with PDPN); arrows indicate WT1 expression in non-epicardial cells. Epi, epicardium; myo, myocardium. Whole heart scale bars, 200μm; high magnification scale bars,100μm. n=4 hearts per group. Data presented as median, IQR and upper and lower limits. Data analysed by Student's t-test **p<0.01. (f) Representative images of immunostaining for CD31 (green), SM-MHC (red) and DAPI (blue) on transverse apical sections of hearts from CTR and KO hearts at 4dpi. Images in top right corner represent high magnifications of boxed region. n=4 hearts per group. RV= right ventricle, LV= left ventricle. Scale bars, 200μm, high magnification scale bars, 50μm. (g) Masson's Trichrome stained transverse sections to show cardiac fibrosis (blue) at 21dpi. * denotes suture placement. Scale bars, 1mm. n=3 for Phd2fl/fl, n=1 for Rosa26+/CreERT2;Phd2fl/fl.

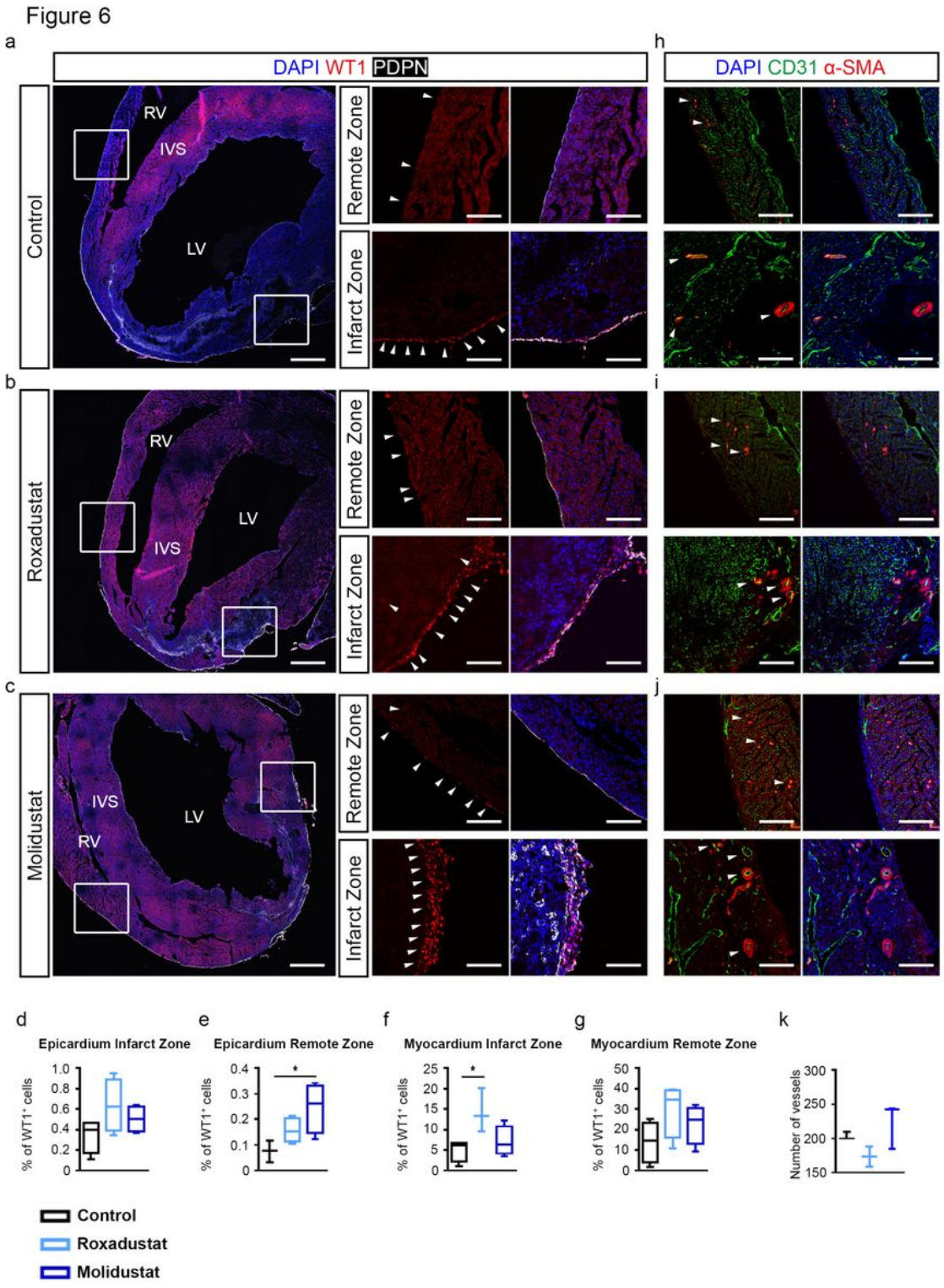

Figure 6

Pharmacological treatment with PHD inhibitors induces WT1 expression. (a) Representative images of immunostaining for WT1 (red), PDPN (white) and DAPI nuclear 8 stain (blue) on sections of hearts from animals treated with either (a) saline (Control), (b) Roxadustat (FG-4592) or (c) Molidustat (BAY 85-3934) and (d-g) quantification of number of WT1 positive cells at 9 days post-injury (dpi). Images on the right represent high magnification views of boxed regions shown in whole heart images. Arrowheads indicate

expression of WT1 in the epicardium (determined by co-expression with PDPN). Whole heart scale bars, 200μm; high magnification scale bars, 100μm. n=4 hearts per group. (h) Representative images of immunostaining for CD31 (green), α-SMA (red) and DAPI (blue) on sections of hearts from animals treated with either (h) saline (Control), (i) Roxadustat (FG-4592) or (j) Molidustat (BAY 85-3934) and (k) quantification of number of vessels at 9 dpi. n=3 hearts per group. IVS= interventricular septum, RV= right ventricle, LV= left ventricle. Scale bars 200μm, high magnification scale bars, 50μm. Data presented as median, IQR and upper and lower limits. Data analysed by one-way ANOVA with Dunnett's post-hoc test *p<0.05.

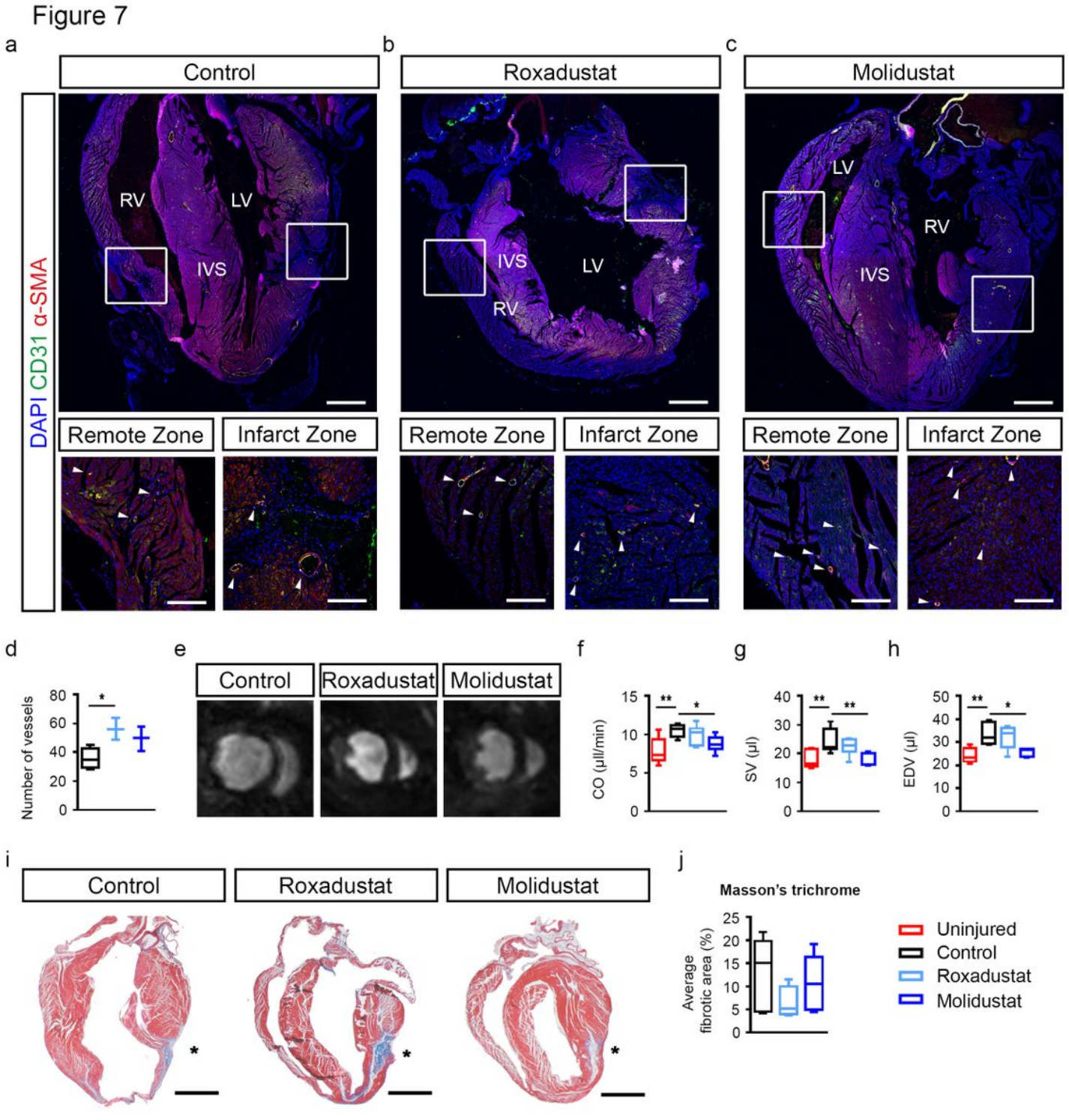

Figure 7

Pharmacological stabilisation of HIF induces new coronary vessel formation and improves heart function. Representative images of immunostaining for α-smooth muscle actin (α-SMA, red), CD31 (green) and DAPI nuclear stain (blue) on sections of hearts from animals treated with either (a) saline (Control), (b) Roxadustat (FG-4592) or (c) Molidustat (BAY 85-3934) and (d) quantification of number of new vessels at 9 days post-injury (dpi). Images below represent high magnification views of boxed regions shown in whole heart images. Arrowheads indicate vessel (determined by co-expression of CD31 and α-SMA). Whole heart scale bars, 200μm; high magnification scale bars,100μm. n=3-4 hearts per group. (e) Representative mid-ventricular short-axis MRI frames for control, Roxadustat and Molidustat treated heart. (f-h) MRI analyses of infarcted control and treated hearts at 21 9 dpi showing reduced CO (f), SV (g), and EDV (h) in Molidustat treated animals, compared 914 with controls. n=5-7 hearts per group. (i) Representative images and (j) quantification of Masson's Trichrome stained transverse sections to show cardiac fibrosis (blue) at 21dpi. * denotes suture placement. Scale bars, 1mm. Data presented as median, IQR and upperand lower limits. Data analysed by one-way ANOVA with Dunnett's post-hoc test *p<0.05, **p<0.01.

Supplementary Files

This is a list of supplementary files associated with this preprint. Click to download.

- SupplementaryInformation.pdf